Multiantenna GLR Detection of Rank-One Signals with Known Power Spectrum under Spatially-Uncorrelated Noise

Josep Sala-Alvarez†,Gonzalo Vazquez-Vilar‡,Roberto López-Valcarce‡†,Saeid Sedighi‡‡, Abbas Taherpour‡‡,

***Abstract*—We establish the generalized likelihood ratio (GLR) test for a Gaussian signal of known power spectrum and unknown rank-one spatial signature in additive Gaussian noise, modeled as temporally white with unknown diagonal spatial correlation matrix. This model is motivated by spectrum sensing problems in Dynamic Spectrum Access (DSA), in which the temporal correlation of the primary signal can be assumed known up to a scale factor and where the noise is due to an uncalibrated array. When the noise is modeled as spatially independent identically distributed (i.i.d.), the corresponding GLR test reduces to a scalar optimization problem, whereas the GLR detector for the general non-i.i.d. case requires solving a more involved problem, which can be done by alternating optimization methods. Low Signal-to-Noise Ratio (SNR) approximations to the detectors are given, together with an asymptotic analysis showing the influence on detection performance of the signal power spectrum and SNR distribution across antennas. Simulation results support our theoretical findings, and show that exploiting prior knowledge about the signal power spectrum can result in significant performance improvement.**

***Index Terms*—GLRT, detection, spectrum sensing, cognitive radio, multiple antenna, uncalibrated array.**

I. Introduction

Array processing for signal detection and parameter estimation has attracted great research interest over the last decades. A rich corpus of techniques has been developed so far for scenarios subject to additive Gaussian noise (see, e.g., [1]–[7]). However, most of these works do not assume prior knowledge about the spectral shape of the signal of interest. In fact, the exploitation of an additional temporal dimension on a sound statistical basis leads to considerable mathematical difficulties, if, in addition, exact expressions are sought [8], [9]. To obtain practical detectors under spatially white noise of known variance, [8] relied on a low-SNR expansion of the Neyman-Pearson detector whereas the exact GLR test (GLRT) has been derived in [9] when the noise is assumed to have no spatial structure. In this work, we obtain the GLRT for the problem of detecting signals with known power spectral density (PSD) in spatially structured noise. In particular, we assume an unknown diagonal form for the spatial correlation matrix of the noise process, either with equal diagonal elements (calibrated receiver) or possibly different (uncalibrated receiver).

These two models emerge in the context of DSA in licensed bands [10], [11]. DSA pursues a more efficient utilization of the available spectrum by allowing access of unlicensed (or *secondary*) users while keeping interference to licensed (or *primary*) users in check. This requires secondary users to have spectrum sensing capabilities [1] as well as access policies [12] for exploiting spectrum holes for transmission. A number of wireless propagation effects such as large- and small-scale fading, the hidden node problem, noise uncertainty, operation in a low-SNR regime, etc. appear in the design and performance of suitable detection schemes. These issues may be tackled, albeit with different effectivity, via cooperative detection (with constraints on the volume of data exchanges between different sensors), and multiantenna detection schemes (with centralized access to all data samples).

Focusing on the latter, previous research into multiantenna detection has combined aspects along the following lines, which exploit different features of the signal model: (i) detectors under a low-rank spatial correlation matrix for the signal of interest; (ii) detectors under different noise spatial correlation models; (iii) detectors exploiting other features of the signal of interest, which may be considered random, unknown deterministic or deterministic. An instance of (iii) are detectors exploiting some type of temporal correlation or frequency domain structure. Popular detection strategies that have been applied are the GLRT, the Locally Most Powerful Invariant Test (LMPIT) and Rao's test (see [13], [14]).

In a brief survey, early work on multiantenna detection was developed in the Radar field. Detection of known signals in unknown noise was treated in [15], [16], and extended later to partially unknown signals in [17]. Motivated by the DSA context, new works have basically considered unknown deterministic or random signals in scenarios subject to unknown parameters of the signal model (e.g. spatial signatures, noise power, etc.), which has resulted somehow in widespread application of the GLRT to avoid detector degradation under parameter uncertainties. Detection of spatially rank-one unknown deterministic signals has been addressed in [18] under spatially i.i.d. noise of unknown variance and in [2] for uncalibrated receivers. For random signals the rank-one case has been approached in [5], [19] (for temporally white signals), and in [8], [9] (for known temporal correlation). Detection of wideband rank-one signals is considered in [20] under spatially uncorrelated noise. All these works attest, explicitly or not, to the complexity of accurately exploiting the spatio-temporal statistical structure of the signal even in the simple rank-one case.

Beyond the rank-one model, LMPIT schemes are studied in [21] for a temporally white signal with an arbitrary rank-deficient spatial correlation whereas [22] exploits spatio-temporal correlations in the received signal. In [23] a single-antenna detector is derived under unknown noise variance using knowledge of the pulse shaping structure. Cyclostationary detectors under a rank-p signal model have been proposed in

Authors affiliation: †Dept. of Signal Theory and Communications, Technical University of Catalonia – Barcelona Tech, Spain; ‡Dept. of Signal Theory and Communications, Universidad Carlos III de Madrid, Spain; ‡†Dept. of Signal Theory and Communications, University of Vigo, Spain; ‡‡Dept. of Electrical Engineering, Imam Khomeini International University (IKIU), Iran.

[24], [25]. Other detectors are also addressed in [26], [27] for spatially white noise; and in [3], [4], [28]–[30] for uncalibrated receivers.

For some licensed services such as broadcast or cellular networks, the (normalized) PSD or emission mask of primary signals is publicly known and may be considered information available to the detector. Following common practice, we adopt a Gaussian model for the primary signal, which is assumed to have an unknown rank-one spatial signature. Thermal noise is modeled as a temporally white additive Gaussian process. In receiver implementations, tolerances in the components of the different radio-frequency (RF) chains originate different per-antenna noise power levels. As a result, several reported detectors are sensitive to these calibration errors [7]. Here, we consider both a scenario in which the noise is spatially white (calibrated receiver), or possibly has distinct noise levels at each antenna (uncalibrated receiver). When the noise is i.i.d., the GLRT is shown to yield a scalar optimization problem, whereas for spatially non-i.i.d. noise a more involved optimization is required. Under certain conditions, the GLRT is shown to adopt a simple closed-form under both noise models.

Organization: The signal model and problem formulation appear in Sec. II. In Sec. III we derive the GLR detectors under both noise models. The asymptotic performance analysis of these tests is presented in Sec. IV. In Sec. V the GLR detectors are particularized under certain signal models. Sec. VI presents a comparative performance analysis and Sec. VII concludes the paper.

Notation: $\mathbb{R}/\mathbb{C}$ refer to the real/complex fields. $\mathbb{E}[\cdot]$ expresses the statistical expectation. Bold lower-/upper-case is used for vectors/matrices. For the $n \times m$ matrix $\boldsymbol{A} \in \mathbb{C}^{n\times m}$, $\boldsymbol{A}^*$, $\boldsymbol{A}^T$, $\boldsymbol{A}^H$ and $\boldsymbol{A}^{-1}$ denote its conjugate, transpose, Hermitian (conjugate transpose) and inverse. $\mathbf{I}_n$ and $\mathbf{0}_{n\times m}$ stand for the $n \times n$ identity and $n \times m$ zero matrices. The reduced Singular Value Decomposition (SVD) of rank-r matrix $\boldsymbol{A} \in \mathbb{C}^{n\times m}$ with $n \leq m$ is $\boldsymbol{A} = \boldsymbol{U}\boldsymbol{S}\boldsymbol{V}^H$, with $\boldsymbol{U} \in \mathbb{U}^{n\times r}, \boldsymbol{V} \in \mathbb{U}^{m\times r}$ semi-unitary matrices and $\boldsymbol{S}$ a $r\times r$ positive diagonal matrix. $\otimes$ denotes Kronecker's product. $\mathrm{tr}(\cdot), \det(\cdot)$ denote the trace and determinant. For a vector $\mathbf{x}$, $\mathrm{diag}(\mathbf{x})$ denotes the diagonal matrix with diagonal equal to $\mathbf{x}$; for a matrix $\mathbf{X}$, $\mathrm{diag}(\mathbf{X})$ denotes the diagonal matrix with diagonal equal to that of $\mathbf{X}$. $\lambda_{\max/\min}[\boldsymbol{A}]$ and $\boldsymbol{e}_{\max/\min}[\boldsymbol{A}]$ are used for the max./min. eigenvalue of $\boldsymbol{A}$ and its associated eigenvector. $\log(\cdot)$ denotes base-e's logarithm.

II. Problem Formulation

The sensor has M antennas with their respective RF chains. The same primary channel is selected at all antennas, down-converted to baseband and I&Q channels are sampled at rate $f_s = 1/T_s$. The resulting M complex signal samples at time kT_s are arranged into the vector $\mathbf{y}_k = s_k\mathbf{h} + \mathbf{n}_k$, where $\mathbf{h} \doteq [h_1, \cdots, h_M]^T$ denotes the vector of complex channel gain coefficients, $s_k \doteq s(kT_s)$ the transmitted baseband signal sample, and $\mathbf{n}_k$ the received complex noise vector, with $\mathbf{n}_k \doteq [n_1(kT_s), \cdots, n_M(kT_s)]^T$. Using Kronecker's product, we stack N consecutive array snapshots $\mathbf{y}_k$ to express the received signal,

$$\mathbf{y} = \mathbf{s} \otimes \mathbf{h} + \mathbf{n}, \tag{1}$$

where $\mathbf{s} \doteq [s_1, \cdots, s_N]^T$ denotes the temporal transmitted signal vector and $\mathbf{y} \doteq [\mathbf{y}_1^T, \cdots, \mathbf{y}_N^T]^T$ and $\mathbf{n} \doteq [\mathbf{n}_1^T, \cdots, \mathbf{n}_N^T]^T$ the received signal and noise stacked vectors, respectively. This model assumes that the channel from the primary transmitter to the spectrum monitor is frequency-flat in the RF channel bandwidth, and that it remains constant for the duration of the sensing interval NT_s.

In the following both signal $\mathbf{s}$ and noise $\mathbf{n}$ are assumed zero-mean complex circular Gaussian. This is a good approximation for Orthogonal Frequency Division Multiplexing (OFDM) signals with a sufficiently large number of subcarriers. For other statistical distributions of $\mathbf{s}$, note that estimators/detectors based on the Gaussian assumption usually lead to sufficient statistics that are sample moments of the data $\mathbf{y}$. It is also known that, regardless of the underlying statistical distribution of $\mathbf{y}$, its sample moments converge to a Gaussian distribution if the data have finite fourth-order moments [31]. In addition, it has been shown that for second-order estimation problems in the low-SNR regime, a Gaussian distribution with second-order moments matching those of the true distribution is a valid alternative [32]. Altogether, it would seem possible that at low SNR the derived detectors achieve competitive performance even if the signal is non-Gaussian. This will be validated later in the simulations section.

We let $\mathbf{C} \doteq \mathbb{E}[\mathbf{s}\mathbf{s}^H]$ denote the $N \times N$ temporal correlation matrix of the primary signal with normalized trace $\frac{1}{N}\,\mathrm{tr}\,\mathbf{C} = 1$. As discussed in Section I, $\mathbf{C}$ is assumed known to the spectral monitor. The noise process $\mathbf{n}$ is modeled as temporally white Gaussian and statistically independent of the transmitted signal. The $M \times M$ spatial correlation matrix of the noise process is denoted as $\boldsymbol{\Sigma}^2 \doteq \mathbb{E}[\mathbf{n}_k\mathbf{n}_k^H]$. Then, the $MN \times MN$ covariance matrix of the received signal becomes

$$\mathbf{R}_y \doteq \mathbb{E}[\mathbf{y}\mathbf{y}^H] = \mathbf{I}_N \otimes \boldsymbol{\Sigma}^2 + \mathbf{C} \otimes \mathbf{h}\mathbf{h}^H. \tag{2}$$

We will conduct a comparative analysis under the following models for $\boldsymbol{\Sigma}^2$:

- **Model 1**: Calibrated system with equal noise powers at each of the antennas. This system corresponds to spatially i.i.d. (or *spatially white*) noise, i.e.,

  $$\boldsymbol{\Sigma}^2 = \sigma^2\mathbf{I}_M. \tag{3}$$

  This model was considered in [8] under the assumption of a known noise variance σ^2, and in [5] for $\mathbf{C} = \mathbf{I}_N$ (temporally white signal) and σ^2 unknown.
- **Model 2**: System with uncalibrated radio-frequency (RF) front-ends or when receiver antennas are not co-located. This system corresponds to *spatially uncorrelated* noise and it is modeled by $\boldsymbol{\Sigma}^2$ being a diagonal matrix, i.e.,

  $$\boldsymbol{\Sigma}^2 = \mathrm{diag}\big([\sigma_1^2, \ldots, \sigma_M^2]^T\big). \tag{4}$$

  This model was considered in [4], [7] for the case $\mathbf{C} = \mathbf{I}_N$.
- **Model 3**: *Spatially correlated* noise or broadband interference ($\boldsymbol{\Sigma}^2$ an arbitrary full-rank positive definite

matrix). This model has been treated in [9] and will be used here only in comparison with the previous models.

From the Gaussian assumption, the parametrized probability density function (p.d.f.) of the data in terms of the covariance matrix $\mathbf{R}_y$ is given by,

$$f(\mathbf{y}\,|\,\mathbf{R}_y) \;=\; \frac{\exp\left(-\mathbf{y}^H\mathbf{R}_y^{-1}\mathbf{y}\right)}{\pi^{MN}\det\mathbf{R}_y}, \tag{5}$$

which depends on the unknown parameters $\mathbf{h}$ and $\boldsymbol{\Sigma}^2$ through $\mathbf{R}_y$ as stated in (2).

We are interested in determining the presence or absence of the signal from an observation $\mathbf{y}$. The corresponding hypothesis test can be written in terms of the covariance matrix $\mathbf{R}_y$ as

$$\mathcal{H}_0:\ \mathbf{R}_y \;=\; \mathbf{I}_N\otimes\boldsymbol{\Sigma}^2 \;\doteq\; \mathbf{R}_0, \tag{6}$$

$$\mathcal{H}_1:\ \mathbf{R}_y \;=\; \mathbf{I}_N\otimes\boldsymbol{\Sigma}^2+\mathbf{C}\otimes\mathbf{h}\mathbf{h}^H \;\doteq\; \mathbf{R}_1. \tag{7}$$

Since $\mathbf{h}$ and $\boldsymbol{\Sigma}^2$ are unknown, a sensible approach is the GLRT. In the GLRT, the unknown parameters in the likelihood ratio are substituted by their Maximum Likelihood (ML) estimates under each hypothesis, yielding

$$T \doteq \frac{\max_{\mathbf{R}_1} f(\mathbf{y}\,|\,\mathbf{R}_1)}{\max_{\mathbf{R}_0} f(\mathbf{y}\,|\,\mathbf{R}_0)} \underset{\mathcal{H}_0}{\overset{\mathcal{H}_1}{\gtrless}} \gamma, \tag{8}$$

where $\gamma>1$ is a suitable threshold.

This test will be established under Models 1, 2 and 3 for $\boldsymbol{\Sigma}^2$. Note that $\boldsymbol{\Sigma}^2$ under model m subsumes $\boldsymbol{\Sigma}^2$ under models $m'<m$, so that the corresponding detector will be capable to operate under the previous noise models (although with possibly different performance).

III. GLR Detectors

To derive the ML estimates under both hypotheses, we first express the log-likelihood,

$$\log f(\mathbf{y}\,|\,\mathbf{R}_y) = -\mathbf{y}^H\mathbf{R}_y^{-1}\mathbf{y} - MN\log\pi - \log\det\mathbf{R}_y, \tag{9}$$

in a more convenient form. We will only operate with $\mathbf{R}_y=\mathbf{R}_1$ under $\mathcal{H}_1$, as, setting $\mathbf{h}=\mathbf{0}_M$, yields the corresponding expressions under $\mathcal{H}_0$.

Using a generalization of Sylvester's determinant identity to Kronecker products [33], in view of (2), we can rewrite the determinant term in (9) as

$$\log\det\mathbf{R}_y \;=\; N\log\det\left(\boldsymbol{\Sigma}^2\right)+\log\det(\mathbf{I}_N+\rho\mathbf{C}), \tag{10}$$

where the parameter $\rho\doteq\mathbf{h}^H\boldsymbol{\Sigma}^{-2}\mathbf{h}$ corresponds to the SNR at the output of the Capon beamformer $\mathbf{w}\doteq\boldsymbol{\Sigma}^{-2}\mathbf{h}$ when signal $\mathbf{s}$ is unit-power. The inverse of the received signal covariance matrix can also be written as [9],

$$\mathbf{R}_y^{-1} = \mathbf{I}_N\otimes\boldsymbol{\Sigma}^{-2}-\mathbf{C}(\rho)\otimes\left(\boldsymbol{\Sigma}^{-1}\mathbf{h}\mathbf{h}^H\boldsymbol{\Sigma}^{-1}\right), \tag{11}$$

$$\mathbf{C}(\rho)\doteq\mathbf{C}(\mathbf{I}_N+\rho\mathbf{C})^{-1}. \tag{12}$$

Then, using the identity $\mathrm{tr}(\mathbf{A}^T\mathbf{B}^H\mathbf{C}\,\mathbf{D}) = \mathrm{vec}(\mathbf{B})^H(\mathbf{A}\otimes\mathbf{C})\,\mathrm{vec}(\mathbf{D})$, straightforward algebra yields,

$$\begin{aligned}&\mathbf{y}^H\mathbf{R}_1^{-1}\mathbf{y}\\ &\;=\;\mathrm{tr}\left(\boldsymbol{\Sigma}^{-2}\mathbf{Y}\mathbf{Y}^H\right)-\mathrm{tr}\left(\boldsymbol{\Sigma}^{-2}\mathbf{h}\mathbf{h}^H\boldsymbol{\Sigma}^{-2}\mathbf{Y}\mathbf{C}^*(\rho)\mathbf{Y}^H\right),\end{aligned} \tag{13}$$

where, for convenience, we defined the $M\times N$ data matrix

$$\mathbf{Y}\doteq\left[\mathbf{y}_1\,\cdots\,\mathbf{y}_N\right]. \tag{14}$$

Substituting (10) and (13), the log-likelihood (9) becomes,

$$\begin{aligned}&\log f(\mathbf{Y}\,|\,\mathbf{h},\boldsymbol{\Sigma}^2)\\ &\;=\;-MN\log\pi-N\log\det\boldsymbol{\Sigma}^2-\log\det(\mathbf{I}_N+\rho\mathbf{C})\\ &\;-\mathrm{tr}\left(\boldsymbol{\Sigma}^{-2}\mathbf{Y}\mathbf{Y}^H\right)+\mathrm{tr}\left(\boldsymbol{\Sigma}^{-2}\mathbf{h}\mathbf{h}^H\boldsymbol{\Sigma}^{-2}\mathbf{Y}\mathbf{C}^*(\rho)\mathbf{Y}^H\right),\end{aligned} \tag{15}$$

where ρ depends on $\mathbf{h}$ and $\boldsymbol{\Sigma}^2$ as $\rho=\mathbf{h}^H\boldsymbol{\Sigma}^{-2}\mathbf{h}$. We next optimize this expression under $\mathcal{H}_0$ and $\mathcal{H}_1$ to obtain the GLR test corresponding to each of the three models described in Section II.

A. Spatially white noise

First, assume that the noise is i.i.d., that is, $\boldsymbol{\Sigma}^2$ is a scaled version of the identity matrix (Section II, Model 1). The next result shows that the normalized data matrix,

$$\bar{\mathbf{Y}}\doteq\frac{\mathbf{Y}}{\sqrt{\mathrm{tr}\left(\mathbf{Y}\mathbf{Y}^H\right)}}, \tag{16}$$

is a sufficient statistic for GLR detection under this model.

Theorem 1 (GLRT under Model 1): The GLR test statistic under *spatially white* (sw) noise, i.e., when $\boldsymbol{\Sigma}^2=\sigma^2\mathbf{I}_M$, is

$$T_{\text{sw}} = \max_{\rho\geq 0}\ t_{\text{sw}}(\rho), \tag{17}$$

$$t_{\text{sw}}(\rho)\doteq\frac{\left(1-\rho\lambda_{\max}\left(\bar{\mathbf{Y}}\mathbf{C}^*(\rho)\bar{\mathbf{Y}}^H\right)\right)^{-MN}}{\det(\mathbf{I}_N+\rho\mathbf{C})}. \tag{18}$$

Proof: See Appendix A-1. ∎

The value of ρ maximizing $t_{\text{sw}}(\rho)$ cannot be expressed in closed form, except in certain cases. For white primary signals, i.e. $\mathbf{C}=\mathbf{I}_N$, (17) is equivalent to the test statistic $\lambda_{\max}(\bar{\mathbf{Y}}\bar{\mathbf{Y}}^H)=\frac{\lambda_{\max}(\mathbf{Y}\mathbf{Y}^H)}{\mathrm{tr}(\mathbf{Y}\mathbf{Y}^H)}$, recovering the result in [5].

In the low-SNR regime, we may derive a GLR detector equivalent to (17) by considering the first coefficient of the Taylor series expansion of $\log t_{\text{sw}}(\rho)$ as $\rho\to 0^+$. In Appendix A-2 it is shown that T_{sw} yields the following equivalent low-SNR closed-form test,

$$\Lambda_{\text{sw}}^{\text{low}}\doteq\max\left\{0,\ \lim_{\rho\to 0^+}\frac{1}{\rho}\log t_{\text{sw}}(\rho)\right\} \tag{19}$$

$$=\left[\,NM\lambda_{\max}\left(\bar{\mathbf{Y}}\mathbf{C}^*\bar{\mathbf{Y}}^H\right)-\mathrm{tr}\,\mathbf{C}^*\,\right]^+, \tag{20}$$

where $[x]^+\doteq\max\{0,x\}$. Note that $\Lambda_{\text{sw}}^{\text{low}}$ does not depend on ρ, as desired.

B. Spatially uncorrelated noise

When the noise is assumed independent across antennas, but not identically distributed, $\boldsymbol{\Sigma}^2$ is modeled as an arbitrary positive-definite diagonal matrix (Section II, Model 2). In this case, the derivation of the GLRT is more involved and cannot be reduced to a scalar optimization problem.

Let $\mathbf{D}^2$ denote the diagonal component of the sample correlation matrix $\frac{1}{N}\mathbf{Y}\mathbf{Y}^H$, i.e.,

$$\mathbf{D}^2\doteq\frac{1}{N}\mathrm{diag}\left(\mathbf{Y}\mathbf{Y}^H\right). \tag{21}$$

Under $\mathcal{H}_0$, $\mathbf{h}=\mathbf{0}$ and the ML estimate of the noise covariance $\mathbf{\Sigma}^2$ yields $\mathbf{D}^2$. Substituting $\mathbf{h}=\mathbf{0}$ and $\mathbf{\Sigma}^2=\mathbf{D}^2$ in (15), we obtain the compressed log-likelihood

$$\ell_0 \doteq -MN\log\pi - N\log\det\mathbf{D}^2 - MN. \tag{22}$$

In order to find the ML estimates under $\mathcal{H}_1$, instead of the parameter space $\Omega=\{\mathbf{\Sigma},\mathbf{h}\}$, we find it useful to define a new parameter space $\Omega'=\{\mathbf{T},\overline{\boldsymbol{v}},\rho\}$, with $\rho=\mathbf{h}^H\mathbf{\Sigma}^{-2}\mathbf{h}$ as before, and

$$\mathbf{T} \doteq \mathbf{D}\mathbf{\Sigma}^{-1}, \tag{23}$$

$$\overline{\boldsymbol{v}} \doteq \boldsymbol{v}/\|\boldsymbol{v}\|, \quad \boldsymbol{v}\doteq\mathbf{D}\mathbf{\Sigma}^{-2}\mathbf{h}. \tag{24}$$

It is easy to check that $\|\boldsymbol{v}\|^2=\frac{\rho}{\overline{\boldsymbol{v}}^H\mathbf{T}^{-2}\overline{\boldsymbol{v}}}$. The mapping $\omega:\Omega\to\Omega'$ is bijective, with an inverse mapping $\omega^{-1}:\Omega'\to\Omega$ given by

$$\mathbf{\Sigma} = \mathbf{D}\mathbf{T}^{-1}, \tag{25}$$

$$\mathbf{h} = \sqrt{\frac{\rho}{\overline{\boldsymbol{v}}^H\mathbf{T}^{-2}\overline{\boldsymbol{v}}}}\,\mathbf{T}^{-2}\mathbf{D}\overline{\boldsymbol{v}}. \tag{26}$$

Hence, it is equivalent to optimize the log-likelihood either over Ω or over Ω'. This new parameter space will allow us to derive explicit expressions for the ML estimates under hypothesis $\mathcal{H}_1$.

Let us define the normalized data matrix,

$$\tilde{\mathbf{Y}} \doteq \mathbf{D}^{-1}\mathbf{Y}. \tag{27}$$

Using (25)-(26) and (27) we write (15) as a function of the new parameter space Ω',

$$\begin{aligned}&\log f\big(\tilde{\mathbf{Y}}\,|\,\mathbf{T},\overline{\boldsymbol{v}},\rho\big)\\ &= -MN\log\pi + N\log\det\left(\mathbf{D}^{-2}\mathbf{T}^2\right) - \log\det(\mathbf{I}_N+\rho\mathbf{C})\\ &\quad - N\,\mathrm{tr}\left(\mathbf{T}^2\right) + \frac{\rho}{\overline{\boldsymbol{v}}^H\mathbf{T}^{-2}\overline{\boldsymbol{v}}}\,\mathrm{tr}\left(\overline{\boldsymbol{v}}^H\tilde{\mathbf{Y}}\mathbf{C}^*(\rho)\tilde{\mathbf{Y}}^H\overline{\boldsymbol{v}}\right).\end{aligned} \tag{28}$$

Using (22) and (28), we write the log-likelihood ratio as

$$\begin{aligned}\Lambda\big(\tilde{\mathbf{Y}}\,|\,\mathbf{T},\overline{\boldsymbol{v}},\rho\big) &\doteq \log f\big(\tilde{\mathbf{Y}}\,|\,\mathbf{T},\overline{\boldsymbol{v}},\rho\big) - \ell_0 \qquad (29)\\ &= -\log\det(\mathbf{I}_N+\rho\mathbf{C})\\ &\quad + N\left(\log\det\left(\mathbf{T}^2\right) - \mathrm{tr}\left(\mathbf{T}^2\right) + M + \frac{\beta(\overline{\boldsymbol{v}},\rho)}{\overline{\boldsymbol{v}}^H\mathbf{T}^{-2}\overline{\boldsymbol{v}}}\right), \qquad (30)\end{aligned}$$

where we defined

$$\beta(\overline{\boldsymbol{v}},\rho) \doteq \frac{\rho}{N}\overline{\boldsymbol{v}}^H\tilde{\mathbf{Y}}\mathbf{C}^*(\rho)\tilde{\mathbf{Y}}^H\overline{\boldsymbol{v}}. \tag{31}$$

The next result provides the expression for the maximizing $\mathbf{T}$ in terms of ρ and $\overline{\boldsymbol{v}}$.

Proposition 1: Let $\mathbf{T}(\overline{\boldsymbol{v}},\rho)=\mathrm{diag}\,[t_1,\ldots,t_M]$ maximize (30) for $\overline{\boldsymbol{v}}$ and ρ given. Then,

$$t_i^2 = \frac{1+\sqrt{1+|\overline{v}_i|^2q^2\big(\sqrt{\beta(\overline{\boldsymbol{v}},\rho)}\big)}}{2}, \tag{32}$$

where $q(\tau)$ is the inverse of the function

$$\begin{aligned}\tau(q) &\doteq \frac{1}{q}\sum_{i=1}^{M}\left(\sqrt{1+q^2|\overline{v}_i|^2}-1\right) \qquad (33)\\ &= q\sum_{i=1}^{M}\frac{|\overline{v}_i|^2}{1+\sqrt{1+q^2|\overline{v}_i|^2}}, \qquad (34)\end{aligned}$$

which depends implicitly on $\overline{\boldsymbol{v}}$.

Moreover, for $\mathbf{T}$ equal to $\mathbf{T}(\overline{\boldsymbol{v}},\rho)$ it holds that

$$\frac{\beta(\overline{\boldsymbol{v}},\rho)}{\overline{\boldsymbol{v}}^H\mathbf{T}^{-2}\overline{\boldsymbol{v}}} = \mathrm{tr}\big(\mathbf{T}^2\big) - M. \tag{35}$$

Proof: See Appendix B-1. ∎

Substituting (35) in (30) we obtain the following expression for the GLRT as an optimization over the compressed space $\Omega'_-=\{\overline{\boldsymbol{v}},\rho\}$.

Theorem 2 (GLRT under Model 2): The GLR test statistic under *spatially uncorrelated* (su) noise, is given by the following optimization problem over the parameters $\{\overline{\boldsymbol{v}},\rho\}$,

$$T_{\text{su}} = \max_{\rho\geq 0,\|\overline{\boldsymbol{v}}\|=1} t_{\text{su}}(\overline{\boldsymbol{v}},\rho), \tag{36}$$

$$t_{\text{su}}(\overline{\boldsymbol{v}},\rho) \doteq \frac{\det^N[\mathbf{T}^2(\overline{\boldsymbol{v}},\rho)]}{\det\left(\mathbf{I}_N+\rho\mathbf{C}\right)}. \tag{37}$$

where the value of $\mathbf{T}(\overline{\boldsymbol{v}},\rho)$ depends on $\overline{\boldsymbol{v}},\rho$ as stated in Proposition 1.

In contrast with Model 1, for which the GLR detector could be reduced to a scalar optimization problem, the detector under Model 2 is formulated as an optimization problem in $\{\overline{\boldsymbol{v}},\rho\}$. In particular, in Model 1, the inner maximization over $\overline{\boldsymbol{v}}$ corresponds to the computation of the eigenvector associated to the extreme eigenvalue of a given matrix. This is not the case under Model 2.

In order to compute the test statistic in (36) we need to solve a joint optimization problem over the variables ρ and $\overline{\boldsymbol{v}}$. Since $t_{\text{su}}(\overline{\boldsymbol{v}},\rho)$ is a non-convex function, the optimization in (36) cannot be solved in closed-form in general. Alternatively, Algorithm 1 proposes an iterative procedure that approximates (36). Algorithm 1 sequentially maximizes (30) over $\{\overline{\boldsymbol{v}},\rho\}$ assuming $\mathbf{T}$ fixed, and then over $\mathbf{T}$ assuming $\{\overline{\boldsymbol{v}},\rho\}$ fixed. Since at each step the objective (30) cannot decrease, this alternating optimization scheme converges to a stationary point. While there are no guarantees that the global maximum in (36) is attained, Algorithm 1 shows a good performance in practice under several system models as it will be shown in Section VI.

Proceeding analogously to the derivation of (20), Theorem 2 yields the following equivalent low-SNR test (see Appendix B-2 for a rigorous derivation)

$$\Lambda_{\text{su}}^{\text{low}} \doteq \Big[\,\lambda_{\max}\big(\tilde{\mathbf{Y}}\mathbf{C}^*\tilde{\mathbf{Y}}^H\big) - \mathrm{tr}\,\mathbf{C}^*\,\Big]^+. \tag{38}$$

Setting $\mathbf{C}=\mathbf{I}_N$ in (38) and disregarding the data-independent terms, we recover the low-SNR detector $\lambda_{\max}\big(\tilde{\mathbf{Y}}\tilde{\mathbf{Y}}^H\big) = \lambda_{\max}\big(\mathbf{D}^{-1}\mathbf{Y}\mathbf{Y}^H\mathbf{D}^{-1}\big)$ derived in [7] for temporally white primary signals. Other particular scenarios in which the detector T_{su} can be simplified will be discussed in Section V.

C. Spatially correlated noise

Finally, let us assume that $\mathbf{\Sigma}^2$ is an arbitrary full-rank positive definite matrix (Section II, Model 3). The GLRT under this model is given in [9] and it is included next for comparison purposes.

Theorem 3 (GLRT under Model 3): Let $\mathbf{Y}=\mathbf{U}\mathbf{S}\mathbf{V}^H$ be the reduced singular value decomposition (SVD) of the data

Algorithm 1 Alternating optimization algorithm to approximate T_{su} in (36). Parameter δ indicates stop criterion.

1) Initialize $k \leftarrow 0$, $\mathbf{T}_0 \leftarrow \mathbf{I}_M$, $T_{\text{su}}^{(0)} \leftarrow 1$.
2) For $\mathbf{T} = \mathbf{T}_k$ maximize (30) with respect to $\{\overline{\boldsymbol{v}}, \rho\}$. We obtain

$$\rho_{k+1} = \arg\max_{\rho \geq 0} \big\{ \rho \lambda_{\max}\big(\mathbf{T}_k \tilde{\mathbf{Y}} \mathbf{C}^*(\rho) \tilde{\mathbf{Y}}^H \mathbf{T}_k\big) - \log\det(\mathbf{I}_N + \rho \mathbf{C}) \big\}. \qquad (\star)$$

Let $\boldsymbol{e}_{\max}$ denote the eigenvector associated to $\lambda_{\max}$ in $(\star)$. Then,

$$\overline{\boldsymbol{v}}_{k+1} = \frac{\mathbf{T}_k \boldsymbol{e}_{\max}}{\|\mathbf{T}_k \boldsymbol{e}_{\max}\|}.$$

3) Update $k \leftarrow k+1$ and compute $\mathbf{T}_k = \mathbf{T}(\rho_k, \overline{\boldsymbol{v}}_k)$ as stated in Proposition 1.
4) We update the objective

$$T_{\text{su}}^{(k)} = \frac{\det^N\big(\mathbf{T}_k^2\big)}{\det\left(\mathbf{I}_N + \rho_k \mathbf{C}\right)}.$$

If $\frac{T_{\text{su}}^{(k)} - T_{\text{su}}^{(k-1)}}{T_{\text{su}}^{(k)}} \leq \delta$, set $T_{\text{su}} \leftarrow T_{\text{su}}^{(k)}$ and finish. Otherwise, go back to step 2).

matrix $\mathbf{Y}$. The GLR test statistic under *spatially correlated* (sc) noise, i.e., when $\boldsymbol{\Sigma}^2$ is assumed arbitrary full-rank positive definite, is

$$T_{\text{sc}} = \max_{\rho \geq 0} \; t_{\text{sc}}(\rho), \qquad (39)$$

$$t_{\text{sc}}(\rho) \doteq \frac{\big(1 - \rho \lambda_{\max}\big(\mathbf{V}^H \mathbf{C}^*(\rho) \mathbf{V}\big)\big)^{-N}}{\det(\mathbf{I}_N + \rho \mathbf{C})}. \qquad (40)$$

In the low-SNR regime, Theorem 3 yields the following equivalent closed-form test

$$\Lambda_{\text{sc}}^{\text{low}} = \left[\, NM \lambda_{\max}\left(\mathbf{V}^H \mathbf{C}^* \mathbf{V}\right) - \text{tr}(\mathbf{C}^*) \,\right]^+. \qquad (41)$$

IV. Performance Analysis

For a given test statistic T and threshold γ in (8), the detection and false-alarm probabilities are defined as

$$P_{\text{D}} = \Pr\big\{T > \gamma \;\big|\; \mathcal{H}_1\big\} \quad , \quad P_{\text{FA}} = \Pr\big\{T > \gamma \;\big|\; \mathcal{H}_0\big\}. \qquad (42)$$

For the tests in Section III, the probabilities in (42) can be approximated for a sufficiently large sample size using the asymptotic distribution of a GLR statistic T_{GLR} which, under suitable conditions [13], is given by

$$2\log T_{\text{GLR}} \overset{\text{under } \mathcal{H}_0}{\sim} \chi_r^2, \quad 2\log T_{\text{GLR}} \overset{\text{under } \mathcal{H}_1}{\sim} \chi_r'^2(\alpha), \qquad (43)$$

with χ_r^2 and $\chi_r'^2(\alpha)$ respectively the central and noncentral chi-square distributions with r degrees of freedom, and noncentrality parameter α. The number of degrees of freedom r is given by the number of real parameters known under hypotheses $\mathcal{H}_0$ and unknown under $\mathcal{H}_1$. In the three models presented, $r = 2M - 1$ as the p.d.f. under $\mathcal{H}_1$ differs from that under $\mathcal{H}_0$ only in $\mathbf{h}\mathbf{h}^H$, i.e., $2M$ real components of $\mathbf{h}$ minus one degree of freedom to account for the invariance to a complex rotation $e^{j\theta}\mathbf{h}$.

The noncentrality parameter α under each noise model can be computed as $\alpha = \mathbb{E}\big[2\log T_{\text{GLR}} \,\big|\, \mathcal{H}_1\big]$. Let "$\rightarrow$" denote convergence as $N \rightarrow \infty$. The asymptotic values of α under the different noise models are derived in Appendix A-3 (Model 1), in Appendix B-3 (Model 2) and in [9, Eq. 74] (Model 3), and yield, respectively,

$$\alpha_{\text{sw}} \rightarrow 2N \log \frac{\left(1 + \frac{\rho}{M}\right)^M}{\det(\mathbf{I}_N + \rho \mathbf{C})^{\frac{1}{N}}}, \qquad (44)$$

$$\alpha_{\text{su}} \rightarrow 2N \log \frac{\prod_{i=1}^M (1 + \rho_i)}{\det(\mathbf{I}_N + \rho \mathbf{C})^{\frac{1}{N}}}, \qquad (45)$$

$$\alpha_{\text{sc}} \rightarrow 2N \log \frac{1 + \rho}{\det(\mathbf{I}_N + \rho \mathbf{C})^{\frac{1}{N}}}, \qquad (46)$$

where $\rho = \mathbf{h}^H \boldsymbol{\Sigma}^{-2} \mathbf{h}$ denotes the (true) overall SNR and $\rho_i \doteq \frac{|h_i|^2}{\sigma_i^2}$ the SNR at the i-th antenna, $i = 1, \ldots, M$.

If the spectrum of the signal of interest $s(t)$ does not contain spectral lines, an equivalent expression can be found in terms of its PSD $P_s(f)$. Let $\mathbf{C} = \mathbf{U}\boldsymbol{\Lambda}\mathbf{U}^H$ be an eigendecomposition of $\mathbf{C}$ with $\boldsymbol{\Lambda} = \text{diag}\big([\lambda_0 \; \lambda_1 \; \cdots \; \lambda_{N-1}]^T\big)$ and $\mathbf{U}$ a $N \times N$ unitary matrix. As $N \rightarrow \infty$ we have the following asymptotic result [34]:

$$\lambda_k \rightarrow P_s(k/N), \quad 0 \leq k \leq N-1. \qquad (47)$$

We define the *spectral uniformity* and *spatial selectivity* coefficients, respectively, as,

$$\xi_t \doteq \left(\int_0^1 P_s^2(f) \mathrm{d}f\right)^{-1}, \quad \xi_s \doteq \sum_{i=1}^M \left(\frac{\rho_i}{\rho}\right)^2 \qquad (48)$$

where $0 < \xi_t \leq 1$ (maximum achieved for a uniform spectrum) and $\frac{1}{M} \leq \xi_s \leq 1$ (minimum achieved for a uniform SNR profile $\rho_i = \frac{\rho}{M}$, $i = 1, \ldots, M$, and maximum for $\rho_m = \rho, \rho_{i \neq m} = 0$). The normalization $\frac{1}{N}\text{tr}(\mathbf{C}) = 1$ implies that $\int_0^1 P_s(f) \mathrm{d}f = 1$.

We denote convergence as $\rho \rightarrow 0^+$ by "$\overset{0}{\rightarrow}$". For small x it follows that $\log(1+x) = x - \frac{1}{2}x^2 + o(x^2)$. Then, using (47), from (44)-(46) we obtain

$$\alpha_{\text{sw}} \rightarrow 2N \left(M \log\left(1 + \frac{\rho}{M}\right) - \int_0^1 \log\big(1 + \rho P_s(f)\big) \mathrm{d}f \right) \qquad (49)$$

$$\overset{0}{\rightarrow} \frac{\rho^2 N}{\xi_t} \left(1 - \frac{\xi_t}{M}\right), \qquad (50)$$

$$\alpha_{\text{su}} \rightarrow 2N \left(\sum_{i=1}^M \log\left(1 + \rho_i\right) - \int_0^1 \log\big(1 + \rho P_s(f)\big) \mathrm{d}f \right) \qquad (51)$$

$$\overset{0}{\rightarrow} \frac{\rho^2 N}{\xi_t} \left(1 - \xi_t \xi_s\right), \qquad (52)$$

$$\alpha_{\text{sc}} \rightarrow 2N \cdot \left(\log\left(1 + \rho\right) - \int_0^1 \log\big(1 + \rho P_s(f)\big) \mathrm{d}f \right) \qquad (53)$$

$$\overset{0}{\rightarrow} \frac{\rho^2 N}{\xi_t} \left(1 - \xi_t\right). \qquad (54)$$

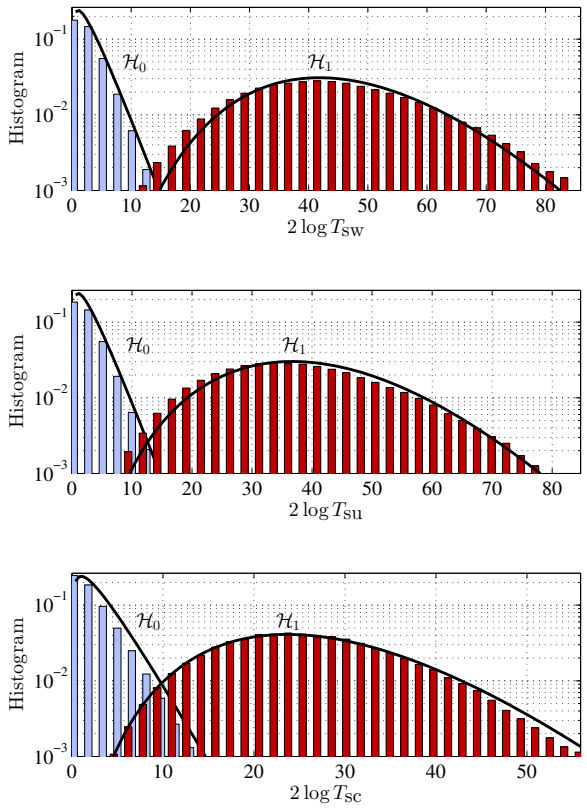

Fig. 1. Theoretical (lines) versus empirical (bars) distributions for a Gaussian primary signal with binary PSD and spatially i.i.d. noise, $M = 2$, $N = 128$, $\rho = -1.5$ dB. The analytical distribution of $2\log T_{\text{su}}$ under $\mathcal{H}_1$ has been averaged over channel realizations.

Given the convexity of $\log(\cdot)$, from Jensen's inequality we obtain

$$\alpha_{\text{sw}} \geq \alpha_{\text{su}} \geq \alpha_{\text{sc}} \qquad (M > 1), \tag{55}$$

$$\alpha_{\text{sw}} = \alpha_{\text{su}} = \alpha_{\text{sc}} \qquad (M = 1). \tag{56}$$

This ordering is intuitively appealing as, for the same ρ and $P_s(f)$, tests under models from 1 to 3 progressively require the estimation of more parameters from the same amount of data. For $M = 1$, the spatial correlation structure under all three noise models is identical, and the performance of the three detectors coincide.

As remarked in [9], for uniform spectrum $P_s(f) = 1$, i.e. $\xi_t = 1$, the detector T_{sc} under spatially correlated noise (Model 3) collapses, and $\alpha_{\text{sc}} = 0$. However, for $M > 1$, detectors T_{sw} and T_{su} do not. This is due to the spatial correlation structure of the noise, which, under Models 1 and 2 warrants that the signal of interest be distinguishable from noise.

While (43) is an asymptotic result, it provides a good approximation to the true statistics of the tests even for moderate sample sizes. Fig. 1 compares the analytical and empirical distributions of the three detectors[1] for a scenario with a Gaussian primary signal with binary PSD occupying half of the bandwidth. In Fig. 1 we can see a good match between the analytical and empirical distributions for a sample size as small as $N = 128$.

[1]For implementation details, see Section VI.

V. Some Particularizations

For some particular scenarios, the GLR tests derived in Section III adopt a simpler form. In this section we particularize these tests (i) for the single antenna case, (ii) under different per-antenna SNR profiles, and (iii) for specific covariance matrices of the primary signal. A summary of the GLR detectors under the three noise models, both in the all-SNR and in the low-SNR regimes can be found in Table I. The parameters of the detectors obtained under a uniform or binary PSD (henceforth binary PSD) are summarized in Table II.

A. Single Antenna

The performance of the GLR detectors under Models 1, 2 and 3, as shown in Section IV, coincide for $M = 1$. Particularizing these detectors and using $\bar{\mathbf{Y}} = \tilde{\mathbf{Y}}/N = \mathbf{V}^H = \frac{\mathbf{y}^T}{\sqrt{\mathbf{y}^H\mathbf{y}}}$ shows that they are indeed the same. In particular, the single antenna GLR test is

$$T_1 \doteq \max_{\rho\geq 0}\ t_1(\rho), \tag{57}$$

$$t_1(\rho) \doteq \frac{\left(1 - \frac{\rho}{\mathbf{y}^H\mathbf{y}}\mathbf{y}^T\mathbf{C}^*(\rho)\mathbf{y}^*\right)^{-N}}{\det(\mathbf{I}_N + \rho\mathbf{C})} = \frac{\left(\frac{1}{\mathbf{y}^H\mathbf{y}}\mathbf{y}^H(\mathbf{I}_N + \rho\mathbf{C})^{-1}\mathbf{y}\right)^{-N}}{\det(\mathbf{I}_N + \rho\mathbf{C})}. \tag{58}$$

In the low SNR regime (57)-(58) yields

$$\Lambda_1^{\text{low}} = \left[\, N\frac{\mathbf{y}^H\mathbf{C}\mathbf{y}}{\mathbf{y}^H\mathbf{y}} - \text{tr}(\mathbf{C}) \,\right]^+. \tag{59}$$

B. Particular per-antenna SNR profiles

Consider the spatially uncorrelated noise model (Section II, Model 2). We shall particularize the detectors T_{su} and its low-SNR equivalent form $\Lambda_{\text{su}}^{\text{low}}$ for different per-antenna SNR profiles. We proceed first with an auxiliary result.

Consider the per-antenna SNR vector $\boldsymbol{\rho} \doteq [\rho_1, \ldots, \rho_M]^T$, with $\rho_i = \frac{|h_i|^2}{\sigma_i^2}$. Using (26), it follows that

$$\rho_i = \frac{|h_i|^2}{\sigma_i^2} = \rho\frac{t_i^{-2}|\overline{v}_i|^2}{\sum_{i=1}^M t_i^{-2}|\overline{v}_i|^2}. \tag{60}$$

We seek to relate ρ_i to $|\overline{v}_i|^2$ in terms of $\beta(\overline{\boldsymbol{v}}, \rho)$ only. The denominator in (60) can be obtained[2] from (100) in Appendix B-1 as $\sum_{i=1}^M t_i^{-2}|\overline{v}_i|^2 = 2\sqrt{\beta(\overline{\boldsymbol{v}}, \rho)}/q\big(\sqrt{\beta(\overline{\boldsymbol{v}}, \rho)}\big)$. Additionally, from Proposition 1, we substitute also t_i^2 in (32) into (60), which allows to relate $|\overline{v}_i|^2$ to ρ_i as follows,

$$\rho_i = \frac{q\big(\sqrt{\beta(\overline{\boldsymbol{v}}, \rho)}\big)}{\sqrt{\beta(\overline{\boldsymbol{v}}, \rho)}}\frac{\rho|\overline{v}_i|^2}{1 + \sqrt{1 + |\overline{v}_i|^2 q^2\big(\sqrt{\beta(\overline{\boldsymbol{v}}, \rho)}\big)}}, \tag{61}$$

in terms of the test parameters $\overline{\boldsymbol{v}}, \rho$, with $\rho_i = \rho_i(\overline{\boldsymbol{v}}, \rho)$.

We next study three particular scenarios in which T_{su} and $\Lambda_{\text{su}}^{\text{low}}$ adopt a simple expression.

[2]We use the fact that the term ϕ in (100) is precisely the implicit function $q\big(\sqrt{\beta(\overline{\boldsymbol{v}}, \rho)}\big)$, as established by (105) and Proposition 1.

1) Single active antenna: Assume that the per-antenna SNR profile follows a delta distribution in which all but the i-th antenna have zero SNR, with i unknown, i.e., $\boldsymbol{\rho} = \rho\boldsymbol{\delta}_i$ with $\boldsymbol{\delta}_i$ the i-th pinning vector.

Substituting $\boldsymbol{\rho} = \rho\boldsymbol{\delta}_i$ in (61), the search over $\overline{\boldsymbol{v}}$ can be constrained to vectors of the form $\overline{\boldsymbol{v}} = e^{j\theta}\boldsymbol{\delta}_i$ where θ is an arbitrary phase term. Setting $\overline{\boldsymbol{v}} = e^{j\theta}\boldsymbol{\delta}_i$ in (34) we obtain $q(\tau) = \frac{2\tau}{1-\tau^2}$. Then, after some algebra, Proposition 1 yields, for $k = 1, \ldots, M$,

$$t_k^2 = \begin{cases} \left(1 - \frac{\rho}{N}\tilde{\mathbf{y}}_i^T\mathbf{C}^*(\rho)\tilde{\mathbf{y}}_i^*\right)^{-1}, & k = i, \\ 1, & k \neq i, \end{cases} \tag{62}$$

with $\tilde{\mathbf{y}}_i^T \doteq \boldsymbol{\delta}_i^T\tilde{\mathbf{Y}}$ the i-th row of $\tilde{\mathbf{Y}}$.

Substituting (62) in (36)-(37), optimizing over vectors of the form $\overline{\boldsymbol{v}} = e^{j\theta}\boldsymbol{\delta}_i$, we obtain the detector

$$T_{\text{su-sc}} \doteq \max_{1\leq i\leq M}\max_{\rho\geq 0} t_{\text{su}}^{(i)}(\rho), \tag{63}$$

$$t_{\text{su}}^{(i)}(\rho) \doteq \frac{\left(1 - \frac{\rho}{N}\tilde{\mathbf{y}}_i^T\mathbf{C}^*(\rho)\tilde{\mathbf{y}}_i^*\right)^{-N}}{\det(\mathbf{I}_N + \rho\mathbf{C})} \tag{64}$$

$$= \frac{\left(\frac{1}{N}\tilde{\mathbf{y}}_i^H(\mathbf{I}_N + \rho\mathbf{C})^{-1}\tilde{\mathbf{y}}_i\right)^{-N}}{\det(\mathbf{I}_N + \rho\mathbf{C})}. \tag{65}$$

That is, the detector simply operates as a *selection combining* (sc) scheme. At low-SNR, i.e., for $\rho \to 0^+$, $T_{\text{su-sc}}$ yields

$$\Lambda_{\text{su-sc}}^{\text{low}} = \left[\max_{1\leq i\leq M}\tilde{\mathbf{y}}_i^H\mathbf{C}\tilde{\mathbf{y}}_i - \operatorname{tr}\mathbf{C}\right]^+. \tag{66}$$

We compare $\Lambda_{\text{su-sc}}^{\text{low}}$ against the selection combining detector in [8, Sec. IV-B, Eq. (24)], which was derived in the low SNR regime for i.i.d. noise with known variance, $\max_{1\leq i\leq M}\bar{\mathbf{y}}_i^H\mathbf{C}\bar{\mathbf{y}}_i$, where $\bar{\mathbf{y}}_i^T = \boldsymbol{\delta}_i^T\mathbf{Y}$ denotes the i-th row of $\mathbf{Y}$. Since $\tilde{\mathbf{y}}_i = N\bar{\mathbf{y}}_i/\|\bar{\mathbf{y}}_i\|$, we can see that, compared to the detector from [8], $\Lambda_{\text{su-sc}}^{\text{low}}$ includes a normalization term due to the lack of knowledge about the noise variances.

2) Uniform per-antenna SNR profile: Assume now that the per-antenna SNR profile is uniform. This may occur for instance when receiving distant sources or under Rice fading, with similar per-antenna signal (and noise) powers. In particular, we assume that $\rho_i = \frac{\rho}{M}$.

Let us define the *equal gain combining* (egc) vectors $\boldsymbol{\psi} \doteq \frac{1}{\sqrt{M}}[e^{j\theta_1}, \cdots, e^{j\theta_M}]^T, 0 \leq \theta_i \leq 2\pi$ for arbitrary phases θ_i, $i = 1, \ldots, M$. From (61) we have that the constraint $\rho_i = \frac{\rho}{M}$ implies $|\overline{v}_i|^2 = \frac{1}{M}$, $i = 1, \ldots, M$. Hence, the optimization over $\overline{\boldsymbol{v}}$ can be replaced by an optimization over the set of egc vectors $\boldsymbol{\psi}$. For $\overline{\boldsymbol{v}} = \boldsymbol{\psi}$, after some algebra, (34) yields $q(\tau) = \frac{2\tau}{1-\tau^2/M}$ and (32) becomes

$$t_i^2 = \left(1 - \frac{\beta(\rho, \boldsymbol{\psi})}{M}\right)^{-1}. \tag{67}$$

Substituting (67) in (36)-(37), and using (31), we obtain the GLR test for a uniform per-antenna SNR profile,

$$T_{\text{su-egc}} = \max_{\rho\geq 0, \boldsymbol{\psi}} t_{\text{su-egc}}(\rho, \boldsymbol{\psi}), \tag{68}$$

$$t_{\text{su-egc}}(\rho, \boldsymbol{\psi}) \doteq \frac{\left(1 - \frac{\rho}{NM}\boldsymbol{\psi}^H\tilde{\mathbf{Y}}\mathbf{C}^*(\rho)\tilde{\mathbf{Y}}^H\boldsymbol{\psi}\right)^{-NM}}{\det(\mathbf{I}_N + \rho\mathbf{C})}. \tag{69}$$

In the low SNR regime as $\rho \to 0^+$, $T_{\text{su-egc}}$ yields

$$\Lambda_{\text{su-egc}}^{\text{low}} \doteq \left[\max_{\boldsymbol{\psi}}\left(\boldsymbol{\psi}^H\tilde{\mathbf{Y}}\mathbf{C}^*\tilde{\mathbf{Y}}^H\boldsymbol{\psi}\right) - \operatorname{tr}\mathbf{C}\right]^+. \tag{70}$$

We compare this detector against the EGC detector in [8, Sec. IV-C], $\max_{\boldsymbol{\psi}}\boldsymbol{\psi}^H\mathbf{Y}\mathbf{C}^*\mathbf{Y}^H\boldsymbol{\psi}$, derived in the low SNR regime for i.i.d. noise with known variance. Again, the noise uncertainty translates into a normalization term via $\tilde{\mathbf{Y}} = \mathbf{D}^{-1}\mathbf{Y}$ in (70).

3) Similar SNR profile: Consider now a small perturbation of the uniform SNR profile $\rho_i = \rho/M$. In particular, assume that $|\overline{v}_i|^2 = \frac{1}{M} + \nu_i$, where ν_i, $i = 1, \ldots, M$, are small perturbations such that $\sum_{i=1}^M \nu_i = 0$.

From (34), and using that for small $|x|$ it holds that $\sqrt{1+x} \simeq 1 + \frac{x}{2}$, it follows that

$$\tau = \frac{1}{q}\sum_{i=1}^M\left(\sqrt{1 + q^2\left(\frac{1}{M} + \nu_i\right)} - 1\right) \tag{71}$$

$$\simeq \frac{1}{q}\sum_{i=1}^M\left(\sqrt{1 + q^2/M} - 1\right) + \frac{1}{2}\sum_{i=1}^M\frac{\nu_i q}{\sqrt{1 + q^2/M}}. \tag{72}$$

Since $\sum_{i=1}^M \nu_i = 0$, the second term in (72) is zero. Therefore, the value of $q(\tau)$ obtained for uniform per-antenna SNR profile is a good approximation to the true $q(\tau)$ (up to second-order). This makes the test $T_{\text{su-egc}}$ in (68) robust to small deviations from the uniform SNR profile. Alternatively to (68), we may leave $\overline{\boldsymbol{v}}$ unconstrained for the maximization, obtaining the *similar gain combiner* (sgc) detector

$$T_{\text{su-sgc}} = \max_{\rho\geq 0} t_{\text{su-sgc}}(\rho), \tag{73}$$

$$t_{\text{su-sgc}}(\rho) \doteq \frac{\left(1 - \frac{\rho}{NM}\lambda_{\max}\left(\tilde{\mathbf{Y}}\mathbf{C}^*(\rho)\tilde{\mathbf{Y}}^H\right)\right)^{-NM}}{\det(\mathbf{I}_N + \rho\mathbf{C})}. \tag{74}$$

This detector has the same form as that in Theorem 1, derived for spatially white noise (Model 1). Note however the different normalization terms, $\bar{\mathbf{Y}} = \mathbf{Y}/\sqrt{\operatorname{tr}(\mathbf{Y}\mathbf{Y}^H)}$ under Model 1 and $\tilde{\mathbf{Y}} = \mathbf{D}^{-1}\mathbf{Y}$ under Model 2. The low-SNR detector corresponding to (74) is precisely $\Lambda_{\text{su-sgc}}^{\text{low}} = \Lambda_{\text{su}}^{\text{low}}$ in (38).

C. Binary power spectrum

Consider a primary signal with *binary power spectrum* (bs), i.e., with power spectrum $P_s(f) \in \{0, S\}$ where $S > 0$ does not depend on f. Using (47), for large N, it follows that the correlation matrix $\mathbf{C}$ can be modeled as $\mathbf{C} = \mu\mathbf{U}_c\mathbf{U}_c^H$, where $\mu = N/r$ is a normalization constant and $\mathbf{U}_c \in \mathbb{C}^{N\times r}$ is semi-unitary, i.e, $\mathbf{U}_c^H\mathbf{U}_c = \mathbf{I}_r$, with r the rank of $\mathbf{C}$. Then,

$$\rho\mathbf{C}(\rho) = \frac{\rho\mu}{1+\rho\mu}\mathbf{U}_c\mathbf{U}_c^H, \tag{75}$$

$$\det(\mathbf{I}_N + \rho\mathbf{C}) = (1+\rho\mu)^r. \tag{76}$$

Using (75)-(76), except for the general detector under spatially uncorrelated noise model (Model 2), the detectors in Table I can be written in the following form,

$$T_{\text{bs}} = \max_{\rho\geq 0}\left\{\frac{\left(1 - \frac{\rho\mu}{1+\rho\mu}b\right)^{-L}}{(1+\rho\mu)^r}\right\}, \tag{77}$$

Spatial Noise Model	Data	all-SNR GLRT (T)	low-SNR GLRT (a_1)
(1) spatially white	$\bar{\mathbf{Y}} = \frac{\mathbf{Y}}{\sqrt{\mathrm{tr}\left(\mathbf{Y}\mathbf{Y}^H\right)}}$	$\max\limits_{\rho\geq 0} \frac{\left(1-\rho\lambda_{\max}\left(\bar{\mathbf{Y}}\mathbf{C}^*(\rho)\bar{\mathbf{Y}}^H\right)\right)^{-NM}}{\det(\mathbf{I}_N+\rho\mathbf{C})}$	$NM\lambda_{\max}\left(\bar{\mathbf{Y}}\mathbf{C}^*\bar{\mathbf{Y}}^H\right) - \mathrm{tr}\,\mathbf{C}$
(2) spatially uncorrelated	$\tilde{\mathbf{Y}} = \mathbf{D}^{-1}\mathbf{Y}$	$\max\limits_{\rho\geq 0,\overline{\boldsymbol{v}}} \frac{\left(\Pi_{k=1}^M t_i^2(\overline{\boldsymbol{v}},\rho)\right)^N}{\det(\mathbf{I}_N+\rho\mathbf{C})}$	$\lambda_{\max}\left(\tilde{\mathbf{Y}}\mathbf{C}^*\tilde{\mathbf{Y}}^H\right) - \mathrm{tr}\,\mathbf{C}$
• Selection Combiner, $\xi_s = 1$	$\tilde{\mathbf{y}}_i^T = \mathrm{row}_i\left(\tilde{\mathbf{Y}}\right)$	$\max\limits_{1\leq i\leq M,\rho\geq 0} \frac{\left(1-\frac{\rho}{N}\tilde{\mathbf{y}}_i^T\mathbf{C}^*(\rho)\tilde{\mathbf{y}}_i\right)^{-N}}{\det(\mathbf{I}_N+\rho\mathbf{C})}$	$\max\limits_{1\leq i\leq M}\left(\tilde{\mathbf{y}}_i^T\mathbf{C}^*\tilde{\mathbf{y}}_i^*\right) - \mathrm{tr}\,\mathbf{C}$
• Eq. Gain Combiner, $\xi_s = \frac{1}{M}$		$\max\limits_{\rho\geq 0,\boldsymbol{\psi}} \frac{\left(1-\frac{\rho}{NM}\boldsymbol{\psi}^H\tilde{\mathbf{Y}}\mathbf{C}^*(\rho)\tilde{\mathbf{Y}}^H\boldsymbol{\psi}\right)^{-NM}}{\det(\mathbf{I}_N+\rho\mathbf{C})}$	$\max\limits_{\boldsymbol{\psi}}\left(\boldsymbol{\psi}^H\tilde{\mathbf{Y}}\mathbf{C}^*\tilde{\mathbf{Y}}^H\boldsymbol{\psi}\right) - \mathrm{tr}\,\mathbf{C}$
• Sim. Gain Combiner, $\xi_s \gtrapprox \frac{1}{M}$		$\max\limits_{\rho\geq 0} \frac{\left(1-\frac{\rho}{NM}\lambda_{\max}\left(\tilde{\mathbf{Y}}\mathbf{C}^*(\rho)\tilde{\mathbf{Y}}^H\right)\right)^{-NM}}{\det(\mathbf{I}_N+\rho\mathbf{C})}$	$\lambda_{\max}\left(\tilde{\mathbf{Y}}\mathbf{C}^*\tilde{\mathbf{Y}}^H\right) - \mathrm{tr}\,\mathbf{C}$
(3) spatially correlated, $\mathbf{C}\neq\mathbf{I}$	$\mathbf{Y} = \mathbf{U}\mathbf{S}\mathbf{V}^H$	$\max\limits_{\rho\geq 0} \frac{\left(1-\rho\lambda_{\max}\left(\mathbf{V}^H\mathbf{C}^*(\rho)\mathbf{V}\right)\right)^{-N}}{\det(\mathbf{I}_N+\rho\mathbf{C})}$	$N\lambda_{\max}\left(\mathbf{V}^H\mathbf{C}^*\mathbf{V}\right) - \mathrm{tr}\,\mathbf{C}$

TABLE I
SUMMARY OF GLR DETECTORS UNDER THE THREE NOISE MODELS, WITH $\Lambda = [a_1]^+$ THE LOW-SNR DETECTOR.

Spatial Noise Model	Data	All-SNR and low-SNR detectors (78) and (79) with parameters:
(1) spatially white	$\bar{\mathbf{Y}}_c = \bar{\mathbf{Y}}\mathbf{U}_c$	$b = \lambda_{\max}\left(\bar{\mathbf{Y}}_c\bar{\mathbf{Y}}_c^H\right),\ L = NM$
(2) spatially uncorrelated	$\tilde{\mathbf{Y}}_c = \tilde{\mathbf{Y}}\mathbf{U}_c$	[no explicit form available]
• Selection Combiner, $\xi_s = 1$	$\tilde{\mathbf{y}}_{c,i}^T = \mathrm{row}_i\left(\tilde{\mathbf{Y}}_c\right)$	$b = \max\limits_{1\leq i\leq M}\left(\frac{1}{N}\tilde{\mathbf{y}}_{c,i}^H\tilde{\mathbf{y}}_{c,i}\right),\ L = N$
• Eq. Gain Combiner, $\xi_s = \frac{1}{M}$		$b = \frac{1}{NM}\max\limits_{\boldsymbol{\psi}}\left(\boldsymbol{\psi}^H\tilde{\mathbf{Y}}_c\tilde{\mathbf{Y}}_c^H\boldsymbol{\psi}\right),\ L = NM$
• Sim. Gain Combiner, $\xi_s \gtrapprox \frac{1}{M}$		$b = \frac{1}{NM}\lambda_{\max}\left(\tilde{\mathbf{Y}}_c\tilde{\mathbf{Y}}_c^H\right),\ L = NM$
(3) spatially correlated, $r\neq N$	$\mathbf{V}_c = \mathbf{U}_c^H\mathbf{V}$	$b = \lambda_{\max}(\mathbf{V}_c\mathbf{V}_c^H),\ L = N$

TABLE II
SUMMARY OF GLR DETECTORS IN TABLE I IN EXPLICIT FORM FOR A BINARY PSD.

where the parameters b and L are specified in Table II for the different noise models. As shown in Appendix C, this optimization can be solved in closed form, yielding

$$T_{\mathrm{bs}} = \max\left\{1, \frac{(r/L)^r(1-r/L)^{L-r}}{b^r(1-b)^{L-r}}\right\}, \tag{78}$$

where the maximum in (77) is attained for $\rho_\star = \frac{1}{\mu r}\max\left\{0, \frac{Lb-r}{1-b}\right\}$.

In the low SNR regime, for the detectors specified in Table II, we have that

$$\Lambda_{\mathrm{bs}}^{\mathrm{low}} = \max\left\{0, Lb-r\right\}. \tag{79}$$

As (78) is non-decreasing in $b\in\left[\frac{r}{L},1\right)$, it follows that both tests (78) and (79) are equivalent. Thus, for the cases considered in Table II, the detectors developed under a low-SNR approximation are in fact equivalent to the all-SNR tests for binary power spectrum. This is not the case, however, for the detector T_{su} and its low-SNR approximation $\Lambda_{\mathrm{su}}^{\mathrm{low}}$, or for general power spectrum densities, as will be shown in Section VI.

VI. SIMULATION RESULTS

We evaluate the performance of the proposed detectors under noise Models 1 and 2. The detector T_{su} has been implemented using Algorithm 1. For all the detectors, the optimization over ρ has been performed using the Newton-Raphson method, with starting point $\rho = 0$.

A. Calibrated vs. uncalibrated receivers

First, we evaluate the performance of the detectors T_{sw}, T_{su} and T_{sc}, and their low-SNR approximations $\Lambda_{\mathrm{sw}}^{\mathrm{low}}$, $\Lambda_{\mathrm{su}}^{\mathrm{low}}$ and $\Lambda_{\mathrm{sc}}^{\mathrm{low}}$ with respect to the SNR. We also compare these results with those predicted by the approximate statistical distributions of the tests presented in Section IV. Consider a Gaussian primary signal with binary PSD occupying half of the bandwidth. For this particular signal, the spectral uniformity coefficient in (48) is $\xi_t = 0.5$. We fix $M = 2$ antennas, $N = 128$ samples.

We perform a Montecarlo simulation with 10^5 averaging iterations for each point in the plot. At each iteration the channel coefficients have been generated from a Rayleigh distribution and normalized to have a constant SNR $\rho = \mathbf{h}^H\boldsymbol{\Sigma}^{-2}\mathbf{h}$. The detection threshold of the different detectors has been chosen

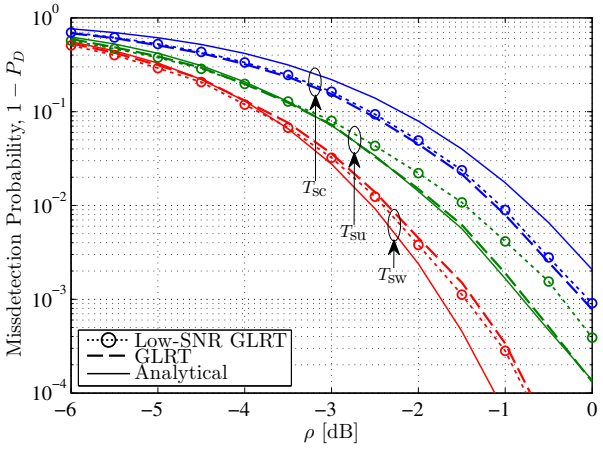

Fig. 2. Gaussian primary signal with binary PSD and spatially i.i.d. noise (Model 1), $M = 2$, $N = 128$, $P_{\text{FA}} = 0.01$.

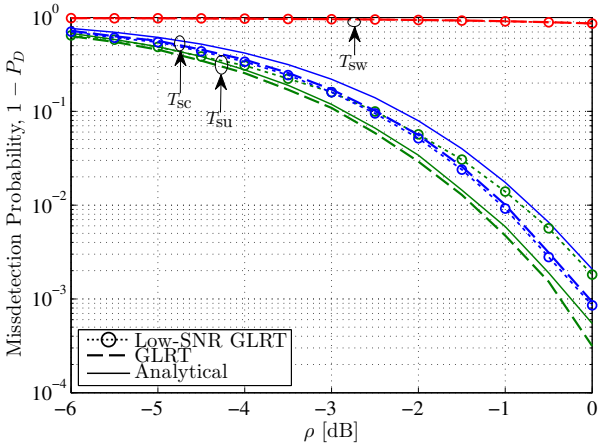

Fig. 3. Gaussian primary signal with binary PSD and spatially uncorrelated noise (Model 2), $M = 2$, $N = 128$, $P_{\text{FA}} = 0.01$.

such that the probability of false alarm under hypothesis $\mathcal{H}_0$ is $P_{\text{FA}} = 0.01$.

Fig. 2 shows the misdetection probability $1 - P_{\text{D}}$ as a function of the SNR ρ when we fix $\mathbf{\Sigma}^2 = \mathbf{I}_2$. This corresponds to the noise Model 1. The detector T_{sw}, derived precisely under the assumption $\mathbf{\Sigma}^2 = \sigma^2\mathbf{I}_2$, shows the best performance. On the other hand, the detectors T_{su} and T_{sc} derived under more general models incur a performance loss. This is in agreement with the results obtained in Section IV for the asymptotic performance of the three detectors.

In Fig. 3 we show the results for same scenario as in Fig. 2, except for the underlying noise model. Here, the diagonal elements of the matrix $\mathbf{\Sigma}^2$ are generated in each iteration according to a χ^2_1 distribution, independently of everything else. This corresponds to the noise Model 2. We can see that whereas the performance of T_{su} and T_{sc} is similar to that in Fig. 2, T_{sw} suffers an important degradation due to the model mismatch. The analytical curve of T_{sw} is not depicted in Fig. 3, since due to the model mismatch analytical expressions are not longer valid. This shows the sensitivity of this detector to calibration errors, a phenomenon also observed in previous detectors in the literature [7].

We note from Fig. 2 and Fig. 3 that the analytical expressions in Section IV approximate the true performance of T_{su} with remarkable accuracy for a sample size as low as $N = 128$, even though those expressions were derived from asymptotic properties of the distributions of the tests.

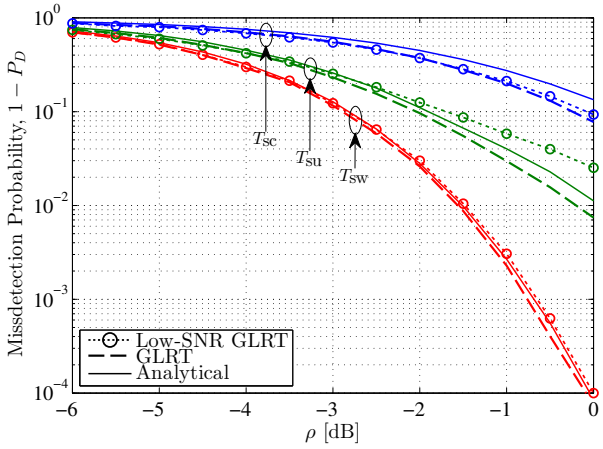

Fig. 4. 16-QAM signal shaped with a squared-root raised cosine filter with roll-off factor 1, for spatially i.i.d. noise (Model 1), $M = 2$, $N = 128$, $P_{\text{FA}} = 0.01$.

B. All-SNR vs. low-SNR detectors

It is interesting to note that in both Figs. 2 and 3, the performance of the all-SNR detector T_{sw} (resp. T_{sc}), and that of the low-SNR detector $\Lambda^{\text{low}}_{\text{sw}}$ (resp. $\Lambda^{\text{low}}_{\text{sc}}$) coincide. This is due to the equivalence of (78) and (79) for binary PSDs. This is however not the case for the GLRT under Model 2, T_{su} and $\Lambda^{\text{low}}_{\text{su}}$, and for other primary signal models. To see this, consider now a 16-QAM primary signal shaped by a square-root raised cosine filter with roll-off factor 1. The receiver bandwidth has been adjusted to the occupied signal bandwidth. All other parameters are as in Fig. 2.

Fig. 4 shows the misdetection probability $1 - P_{\text{D}}$ as a function of the SNR ρ. We can see that, while in this case none of the all-SNR detectors is exactly equivalent to its corresponding low-SNR approximation, the performance loss of the detectors $\Lambda^{\text{low}}_{\text{sw}}$ and $\Lambda^{\text{low}}_{\text{sc}}$ is negligible. We conclude that the closed-form low-SNR detectors offer a good complexity-performance trade-off even when the primary signal PSD is non-binary. We can also see that the proposed detectors are robust to non-Gaussian primary signals.

Comparing Figs. 2 and 4, in Fig. 4 we observe a degradation in the detection probability for the three detectors considered. This performance loss is moderate for T_{sw}, and it becomes increasingly larger for T_{su} and T_{sc}. This can be attributed to the effect of the spectral uniformity coefficient in the different detectors. For the signal considered in Fig. 2, this coefficient is $\xi_t = 0.5$, while for the signal in Fig. 4, $\xi_t \approx 0.67$. From the analysis in Section IV we can see that the asymptotic performance of T_{sw}, T_{su} and T_{sc} depends respectively on the

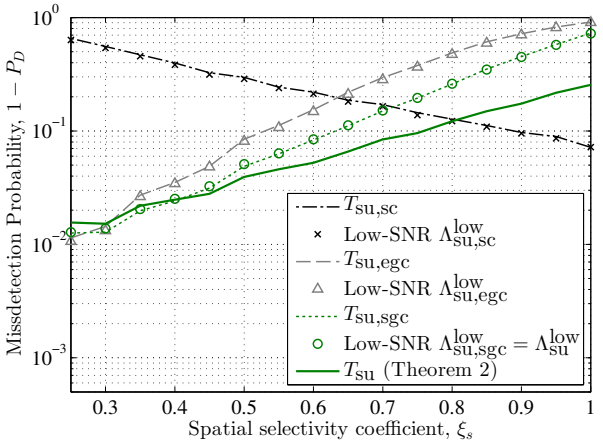

Fig. 5. Gaussian primary signal with binary PSD and spatially uncorrelated noise (Model 2), $\rho = 1$, $M = 4$, $N = 64$, $P_{\text{FA}} = 0.01$.

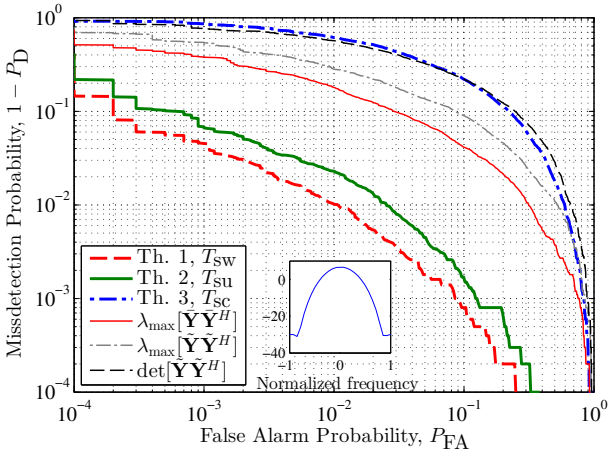

Fig. 6. GMSK primary signal (with PSD shown in the inset) and spatially i.i.d. noise (Model 1), $\rho = 1$, $M = 8$, $N = 64$.

terms $(1 - \xi_t/M)$, $(1 - \xi_t\xi_s)$, $(1 - \xi_t)$, with $\frac{1}{M} \leq \xi_s \leq 1$. Hence these detectors are increasingly sensitive to variations on the uniformity coefficient ξ_t.

Additionally, comparing Figs. 2 and 4, we note that for the 16-QAM scenario in Fig. 4, the performance of T_{su} and T_{sw} is still accurately predicted by the analytical expressions. Complementary results on the analytical performance accuracy of T_{sc} (under spatially correlated noise), may be found in [9].

C. Detector performance vs. spatial selectivity ξ_s

We now evaluate the performance of the detectors derived under Model 2 for particular per-antenna SNR profiles. We consider the GLRT detector T_{su}, and its particularizations: the selection combining detector $T_{\text{su-sc}}$, the equal gain combining detector $T_{\text{su-egc}}$[3], and the similar gain combining detector $T_{\text{su-sgc}}$.

We consider a Gaussian primary signal with binary PSD occupying half of the bandwidth, and a diagonal $\mathbf{\Sigma}^2$. For each simulated point, we fix the per-antenna SNR profile such that ρ_1 and $\rho_i = \rho_0$, $i = 2, \ldots, M$, are chosen to yield the desired spatial selectivity coefficient ξ_s. At each run, the diagonal coefficients of $\mathbf{\Sigma}^2$ are generated according to a χ^2_1 distribution, and the phases of the vector $\mathbf{h}$ are randomly and independently generated from a uniform distribution $\mathcal{U}(0, 2\pi)$. We set $\rho = 1$, $M = 4$, $N = 64$, and we fix $P_{\text{FA}} = 0.01$.

Fig. 5 shows the misdetection probability with respect to the the spatial selectivity coefficient ξ_s. The corresponding low-SNR detectors are shown with markers in the figure. We can see that $T_{\text{su-sc}}$, derived assuming $\xi_s = 1$, outperforms the other detectors when the spatial selectivity coefficient is indeed close to 1. However, its performance degrades rapidly as ξ_s decreases. Whereas the similar gain combining detector $T_{\text{su-sgc}}$ and the equal gain combining detector $T_{\text{su-egc}}$ offer a similar performance in the limit as $\xi_s \to 1/M$, $T_{\text{su-sgc}}$ outperforms

[3]The optimizer of $\boldsymbol{\psi}$ for an objective $\boldsymbol{\psi}^H\mathbf{A}\boldsymbol{\psi}$ has been approximated by using the complex phases of the eigenvector associated to the largest eigenvalue of the matrix $\mathbf{A}$.

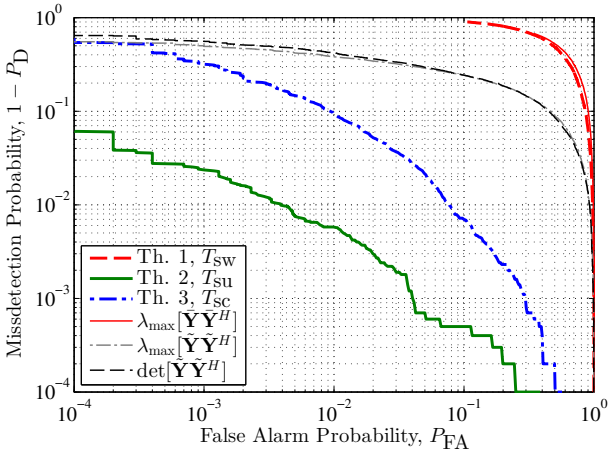

Fig. 7. GMSK primary signal and spatially uncorrelated noise (Model 2), $\rho = 2$, $M = 8$, $N = 64$.

$T_{\text{su-egc}}$ for $\xi_s > 1/M$. For intermediate values of ξ_s the GLRT T_{su} offers the best detection performance.

In Fig. 5 we can see that the performance of the all-SNR detectors $T_{\text{su-sc}}$, $T_{\text{su-egc}}$ and $T_{\text{su-sgc}}$ coincides with that of the corresponding low-SNR detectors, as the signal PSD is binary. Note however, that since $\Lambda^{\text{low}}_{\text{su}} = \Lambda^{\text{low}}_{\text{su-sgc}}$ it does not coincide with that of T_{su}, even for a binary PSD.

D. Comparison with existing detectors for real communication signals

Compared with previous detectors in the literature, the GLR tests presented in Section III exploit prior knowledge of the spectral shape of the signal of interest. To show the advantage of this approach, consider a realistic scenario based on the parameters of the GSM cellular system [35]. We synthesized samples of a baseband Gaussian Minimum Shift Keying (GMSK) waveform based on GSM parameters at a

sampling rate of 400 ksps.[4] At each iteration the channel coefficients have been generated from a Rayleigh distribution and normalized to have a constant SNR $\rho = \mathbf{h}^H \mathbf{\Sigma}^{-2} \mathbf{h}$. We fix $M = 8$ antennas, $N = 64$ samples.

Figures 6 and 7 compare the receiver operating characteristic (ROC) curves of the tests T_{sw}, T_{su} and T_{sc} with respect to existing detectors for a calibrated and an uncalibrated receiver, respectively. In particular, the following base-line tests are considered:

1) GLRT for temporally white Gaussian signals under Model 1 [5], $\lambda_{\max}\big(\bar{\mathbf{Y}}\bar{\mathbf{Y}}^H\big)$. This test was also considered in [18] for an unknown signal, and follows from T_{sw} in (17)-(18) by setting $\mathbf{C} = \mathbf{I}_N$.
2) Low-SNR GLRT for temporally white Gaussian signals under Model 2 [7], $\lambda_{\max}\big(\tilde{\mathbf{Y}}\tilde{\mathbf{Y}}^H\big)$. This test can be also derived from $\Lambda_{\text{su}}^{\text{low}}$ in (38) by setting $\mathbf{C} = \mathbf{I}_N$.
3) Rank-blind GLRT for temporally white Gaussian signals under Model 2 [4], $\det\big(\tilde{\mathbf{Y}}\tilde{\mathbf{Y}}^H\big)$. In [21], this test was shown to be the Locally Most Powerful Invariant Test (LMPIT) at low-SNR when the spatial rank of the primary signal is unknown.

Fig. 6 shows the ROC curves when the noise is spatially i.i.d. (calibrated receiver) and $\rho = 1$. We can see how the proposed tests T_{sw} and T_{su} offer the best performance, whereas the base-line detectors show a detection performance similar to that of T_{sc}. The poor detection performance of T_{sc} in this setting can be attributed to the large number of antennas $M = 8$, given the large number of unknown parameters to be estimated in this case. Fig. 7 shows the ROC curves for a receiver with different noise power levels at each of the antennas and $\rho = 2$. In this setting, the detectors derived under noise Model 1 (namely T_{sw} and $\lambda_{\max}\big(\bar{\mathbf{Y}}\bar{\mathbf{Y}}^H\big)$), suffer an important performance degradation. We can see that T_{su} outperforms the other detectors in this case.

VII. Conclusions

We have derived the generalized likelihood ratio test (GLRT) for detecting Gaussian signals with known temporal correlation and unknown rank-one spatial signature in additive noise, which is assumed to be a temporally-white and spatially-uncorrelated Gaussian process. When the noise is assumed spatially white (i.i.d.), the GLRT is shown to yield a scalar optimization problem. When the noise is assumed spatially non-i.i.d. we have proposed an alternating optimization algorithm to approximate the GLRT.

In the low-SNR regime the GLRT can be obtained in closed-form under both models, and is shown to yield the exact all-SNR GLRT under particular conditions. When the primary signal is assumed temporally white, the proposed GLR tests particularize to several detection schemes in the literature. However, exploiting prior knowledge of the signal temporal correlation significantly improves detection performance. We have provided an accurate asymptotic analysis that quantifies this improvement.

[4]The separation between GSM channels is 200 kHz, although in a given geographical area two adjacent channels cannot be active in order to avoid interference. Thus, the effective channel separation is 400 kHz, which is the same as the approximate bandwidth of the GSM signal. The PSD of the GMSK waveform is shown in the inset in Fig. 6.

Appendix A
GLRT under Model 1

1) Proof of Theorem 1: Under Model 1 we can write $\mathbf{\Sigma}^2 = \sigma^2 \mathbf{I}_M$. Under $\mathcal{H}_0$, i.e. $\mathbf{h} = \mathbf{0}$, the ML estimation of the noise variance $\boldsymbol{\sigma}^2$ yields $\hat{\sigma}_0^2 = \frac{1}{NM}\operatorname{tr}\big(\mathbf{Y}\mathbf{Y}^H\big)$. Substituting $\mathbf{h} = \mathbf{0}$ and $\mathbf{\Sigma}^2 = \hat{\sigma}_0^2 \mathbf{I}_M$ into (15), we obtain the compressed log-likelihood

$$\ell_0 \doteq -MN \log \frac{\pi e}{MN} - MN \log \operatorname{tr}\big(\mathbf{Y}\mathbf{Y}^H\big). \tag{80}$$

Under $\mathcal{H}_1$, we particularize (15) for $\mathbf{\Sigma}^2 = \sigma^2 \mathbf{I}_M$,

$$\begin{aligned}\log f(\mathbf{Y} \,|\, \bar{\mathbf{h}}, \rho, \sigma^2) \;=\; & -MN \log(\pi\sigma^2) - \log\det(\mathbf{I}_N + \rho\mathbf{C}) \\ & - \frac{1}{\sigma^2}\operatorname{tr}\big(\mathbf{Y}\mathbf{Y}^H\big) + \frac{\rho}{\sigma^2}\operatorname{tr}\big(\bar{\mathbf{h}}\bar{\mathbf{h}}^H\mathbf{Y}\mathbf{C}^*(\rho)\mathbf{Y}^H\big), \end{aligned} \tag{81}$$

where $\bar{\mathbf{h}} \doteq \mathbf{h}/\sqrt{\mathbf{h}^H\mathbf{h}}$. The likelihood is now parameterized by $\{\bar{\mathbf{h}}, \rho, \sigma^2\}$.

Setting the derivative of (81) with respect to σ^2 equal to zero, we obtain $\hat{\sigma}_1^2 = \frac{1}{MN}\operatorname{tr}\big(\mathbf{Y}^H\mathbf{Y} - \rho\bar{\mathbf{h}}\bar{\mathbf{h}}^H\mathbf{Y}\mathbf{C}^*(\rho)\mathbf{Y}^H\big)$ for the ML estimate of σ^2 under $\mathcal{H}_1$. Substituting this value into the log-likelihood, we obtain,

$$\begin{aligned}\log f(\mathbf{Y} \,|\, \bar{\mathbf{h}}, \rho) \;=\; & -MN \log \frac{\pi e}{MN} - \log\det(\mathbf{I}_N + \rho\mathbf{C}) \\ & - MN \log\Big(\operatorname{tr}\big(\mathbf{Y}\mathbf{Y}^H\big) - \rho\bar{\mathbf{h}}^H\mathbf{Y}\mathbf{C}^*(\rho)\mathbf{Y}^H\bar{\mathbf{h}}\Big). \end{aligned} \tag{82}$$

The dependence of the likelihood with respect to the unitary vector $\bar{\mathbf{h}}$ is restricted to the term $\bar{\mathbf{h}}^H\mathbf{Y}\mathbf{C}^*(\rho)\mathbf{Y}^H\bar{\mathbf{h}}$. Hence, the maximizing value for $\bar{\mathbf{h}}$ is the eigenvector associated to the largest eigenvalue of the matrix $\mathbf{Y}\mathbf{C}^*(\rho)\mathbf{Y}^H$. Substituting this value into (82), the log-likelihood under $\mathcal{H}_1$ can be written as a scalar optimization problem,

$$\begin{aligned}\ell_1 \doteq \max_{\rho\geq 0}\Big[& -MN \log \frac{\pi e}{MN} - \log\det(\mathbf{I}_N + \rho\mathbf{C}) \\ & -MN \log\big(\operatorname{tr}\big(\mathbf{Y}\mathbf{Y}^H\big) - \rho\lambda_{\max}\big(\mathbf{Y}\mathbf{C}^*(\rho)\mathbf{Y}^H\big)\big)\Big] \end{aligned} \tag{83}$$

Using that $T_{\text{sw}} = \exp\{\ell_1 - \ell_0\}$, the result in Theorem 1 follows.

2) Asymptotic low-SNR GLRT: Consider the Taylor series expansion of $\log t_{\text{sw}}(\rho)$ in Theorem 1 as $\rho \to 0^+$,

$$\log t_{\text{sw}}(\rho) = \sum_{i=1}^{\infty} a_i \rho^i. \tag{84}$$

In the low SNR regime only the coefficient a_1 is relevant for the test (up to first order). In order to compute the coefficient a_1 in the series expansion we use that, as $\rho \to 0^+$,

$$(\mathbf{I}_N + \rho\mathbf{C})^{-1} \;=\; \mathbf{I}_N - \rho\mathbf{C} + o(\rho), \tag{85}$$

$$\det(\mathbf{I}_N + \rho\mathbf{C}) \;=\; 1 + \rho\operatorname{tr}\mathbf{C} + o(\rho) \tag{86}$$

with $o(\rho)$ Landau's "little-o". Substituting (86) in the definition of $t_{\text{sw}}(\rho)$ in (18), applying the logarithm, we obtain

$$\begin{aligned}&\log t_{\text{sw}}(\rho) \\ &= -MN \log\Big(1 - \rho\lambda_{\max}\big(\bar{\mathbf{Y}}\mathbf{C}^*\bar{\mathbf{Y}}^H - \rho\bar{\mathbf{Y}}(\mathbf{C}^*)^2\bar{\mathbf{Y}}^H + o(\rho)\big)\Big) \\ &\quad + \log\big(1 + \rho\operatorname{tr}\mathbf{C}^* + o(\rho)\big) \qquad (87) \\ &= \rho\Big(MN\lambda_{\max}\big(\bar{\mathbf{Y}}\mathbf{C}^*\bar{\mathbf{Y}}^H\big) - \operatorname{tr}\mathbf{C}^*\Big) + o(\rho), \qquad (88)\end{aligned}$$

where we used that $\log(1+a\rho) = a\rho + o(\rho)$. From (88), it follows that the first coefficient in (84) is given by

$$a_1 = MN\lambda_{\max}\left(\bar{\mathbf{Y}}\mathbf{C}^*\bar{\mathbf{Y}}^H\right) - \operatorname{tr}\mathbf{C}^*. \tag{89}$$

For consistency with the maximization range $\rho \geq 0$ in (39), the low-SNR test in (20) is $\max\{0, a_1\}$.

3) Performance analysis: The asymptotic performance of the test T_{sw} is characterized by the non-centrality parameter $\alpha_{\text{sw}} = \mathbb{E}\big[2\log T_{\text{sw}} \,\big|\, \mathcal{H}_1\big]$. To compute this expectation, we recover the property in [9, Eq. 76] concerning convergence in variance when $N \to \infty$,

$$\frac{1}{N}\mathbf{Y}\mathbf{A}\mathbf{Y}^H \overset{\text{var}}{=} \frac{1}{N}\operatorname{tr}(\mathbf{A})\cdot\boldsymbol{\Sigma}^2 + \frac{1}{N}\operatorname{tr}(\mathbf{C}^*\mathbf{A})\cdot\mathbf{h}\mathbf{h}^H. \tag{90}$$

From (90) it follows that, for $N \to \infty$,

$$\mathbf{Y}\mathbf{C}^*(\rho)\mathbf{Y}^H \;\to\; \operatorname{tr}\big(\mathbf{C}^*(\rho)\big)\cdot\boldsymbol{\Sigma}^2 + \operatorname{tr}\big(\mathbf{C}^*\mathbf{C}^*(\rho)\big)\cdot\mathbf{h}\mathbf{h}^H, \tag{91}$$

$$\operatorname{tr}\big(\mathbf{Y}\mathbf{Y}^H\big) \;\to\; NM\sigma^2 + \|\mathbf{h}\|^2\operatorname{tr}\mathbf{C}^*, \tag{92}$$

where we used that $\operatorname{tr}(\boldsymbol{\Sigma}^2) = \operatorname{tr}(\sigma^2\mathbf{I}_M) = M\sigma^2$. From (91) and (92) we obtain

$$\frac{\lambda_{\max}\big(\mathbf{Y}\mathbf{C}^*(\rho)\mathbf{Y}^H\big)}{\operatorname{tr}\big(\mathbf{Y}\mathbf{Y}^H\big)} \to \frac{\sigma^2\operatorname{tr}\big(\mathbf{C}^*(\rho)\big) + \|\mathbf{h}\|^2\operatorname{tr}\big(\mathbf{C}^*\mathbf{C}^*(\rho)\big)}{NM\sigma^2 + \|\mathbf{h}\|^2\operatorname{tr}\mathbf{C}^*}. \tag{93}$$

For λ_k the eigenvalues of $\mathbf{C}$, it follows that

$$\begin{aligned}&\operatorname{tr}\big(\mathbf{C}^*(\rho)\big) + \rho\operatorname{tr}\big(\mathbf{C}^*\mathbf{C}^*(\rho)\big)\\ &= \sum_k \frac{\lambda_k}{1+\rho\lambda_k} + \rho\sum_k \frac{\lambda_k^2}{1+\rho\lambda_k} = \sum_k \lambda_k = \operatorname{tr}\mathbf{C}^*.\end{aligned} \tag{94}$$

Given the consistency of the ML estimator, the estimate of ρ converges to its true value as $N \to \infty$. Then, for $\rho \to \|\mathbf{h}\|^2/\sigma^2$, from (93) and (94) we obtain,

$$\frac{\lambda_{\max}\big(\mathbf{Y}\mathbf{C}^*(\rho)\mathbf{Y}^H\big)}{\operatorname{tr}\big(\mathbf{Y}\mathbf{Y}^H\big)} \;\to\; \frac{\operatorname{tr}\mathbf{C}^*}{NM + \rho\operatorname{tr}\mathbf{C}^*}. \tag{95}$$

Substituting (95) into (17)-(18), yields

$$\alpha_{\text{sw}} \to 2N\log\frac{\big(1+\frac{\rho}{NM}\operatorname{tr}\mathbf{C}^*\big)^M}{\det(\mathbf{I}_N+\rho\mathbf{C})^{\frac{1}{N}}}. \tag{96}$$

In our model, $\operatorname{tr}\mathbf{C}^* = \operatorname{tr}\mathbf{C} = N$. Then, (44) follows.

Appendix B
GLRT under Model 2

1) Proof of Proposition 1: The terms in (30) depending on $\mathbf{T}$ are given by

$$J(\mathbf{T}|\overline{\boldsymbol{v}},\rho) \doteq \log\det\left(\mathbf{T}^2\right) - \operatorname{tr}\left(\mathbf{T}^2\right) + \frac{\beta}{\overline{\boldsymbol{v}}^H\mathbf{T}^{-2}\overline{\boldsymbol{v}}}, \tag{97}$$

with $\beta = \beta(\overline{\boldsymbol{v}},\rho)$. Using that $\mathbf{T}$ is a diagonal matrix, we express $J(\mathbf{T})$ in scalar form as

$$J(\mathbf{T}|\overline{\boldsymbol{v}},\rho) = \sum_{i=1}^M\left(\log t_i^2 - t_i^2\right) + \beta\left(\sum_{i=1}^M |\overline{v}_i|^2 t_i^{-2}\right)^{-1}. \tag{98}$$

Taking the derivative of $J(\mathbf{T}|\overline{\boldsymbol{v}},\rho)$ with respect to t_i^2 yields

$$\frac{\partial}{\partial t_i^2}J(\mathbf{T}|\overline{\boldsymbol{v}},\rho) = t_i^{-2} - 1 + \frac{1}{4}\phi^2|\overline{v}_i|^2 t_i^{-4}, \tag{99}$$

where we defined

$$\phi \doteq 2\sqrt{\beta}\left(\sum_{i=1}^M |\overline{v}_i|^2 t_i^{-2}\right)^{-1}. \tag{100}$$

Equating (99) to zero for each $i = 1,\ldots,M$ we obtain the following nonlinear system of equations

$$t_i^4 - t_i^2 - \frac{1}{4}\phi^2|\overline{v}_i|^2 = 0, \quad i = 1,\ldots,M. \tag{101}$$

The solution of (101) can be shown to be a maximum of $J(\mathbf{T})$. In particular, (101) yields

$$t_i^2 = \frac{1+\sqrt{1+\phi^2|\overline{v}_i|^2}}{2}, \tag{102}$$

where we discarded the negative solution, as t_i^2 must be positive. Note that (102) is an implicit equation since ϕ depends on t_i^2, $i = 1,\ldots,M$. The value of ϕ can be obtained as follows. Substituting (102) in (100) we obtain

$$\phi = 2\sqrt{\beta}\left(\sum_{i=1}^M \frac{2|\overline{v}_i|^2}{1+\sqrt{1+\phi^2|\overline{v}_i|^2}}\right)^{-1} \tag{103}$$

$$= \frac{\sqrt{\beta}\phi^2}{\sum_{i=1}^M\left(\sqrt{1+\phi^2|\overline{v}_i|^2}-1\right)}, \tag{104}$$

where (104) follows from multiplying and dividing by $\sqrt{1+\phi^2|\overline{v}_i|^2}-1$ each of the terms in the sum in (103). Hence, from (104) we obtain that ϕ is defined as an implicit function in terms of β and $\overline{\boldsymbol{v}}$ as

$$\sqrt{\beta} = \frac{1}{\phi}\sum_{i=1}^M\left(\sqrt{1+\phi^2|\overline{v}_i|^2}-1\right). \tag{105}$$

The first part of Proposition 1 follows from (102) and (105).

To prove the second part, we multiply (101) by t_i^{-2} and sum the set of resulting equations for $i = 1,\ldots,M$. We obtain

$$\sum_{i=1}^M\left(t_i^2 - 1\right) = \frac{1}{4}\phi^2\sum_{i=1}^M|\overline{v}_i|^2 t_i^{-2} \tag{106}$$

$$= \beta\left(\sum_{i=1}^M|\overline{v}_i|^2 t_i^{-2}\right)^{-1}, \tag{107}$$

where we used that $\phi^2 = 4\beta\left(\sum_{i=1}^M|\overline{v}_i|^2 t_i^{-2}\right)^{-2}$. Writing the sum in (107) in matrix form, (35) follows.

2) Asymptotic low-SNR GLRT: Let us define

$$\begin{aligned}\lambda_{\text{su}}(\overline{\boldsymbol{v}},\rho) &\doteq \log t_{\text{su}}(\overline{\boldsymbol{v}},\rho)\\ &= N\log\det\big(\mathbf{T}^2(\overline{\boldsymbol{v}},\rho)\big) - \log\det\big(\mathbf{I}_N+\rho\mathbf{C}\big).\end{aligned} \tag{108}$$

The low-SNR GLR detector follows from considering the first term in the low-SNR expansion of $\lambda_{\text{su}}(\overline{\boldsymbol{v}},\rho)$,

$$\Lambda_{\text{su}}^{\text{low}} \doteq \max\left\{0, \max_{\overline{\boldsymbol{v}}}\lim_{\rho\to 0^+}\frac{1}{\rho}\lambda_{\text{su}}(\overline{\boldsymbol{v}},\rho)\right\}. \tag{109}$$

In order to compute $\Lambda_{\text{su}}^{\text{low}}$, we first derive an alternative form for $\lambda_{\text{su}}(\overline{\boldsymbol{v}},\rho)$. By integrating $\tau(q)$ in (34) in Proposition 1 over q, we obtain

$$\int \tau(q)\mathrm{d}q \;=\; \sum_{i=1}^{M}\int \frac{-1+\sqrt{1+|\overline{v}_i|^2q^2}}{q}\mathrm{d}q \tag{110}$$
$$= c+\sum_{i=1}^{M}\left(\sqrt{1+|\overline{v}_i|^2q^2}-\log\left(1+\sqrt{1+|\overline{v}_i|^2q^2}\right)\right),$$

for an arbitrary constant c, where the last step follows from [36, Eq. 17.9.12]. Also from (34) it follows that

$$q\cdot\tau(q)=\sum_{i=1}^{M}\Big(\sqrt{1+q^2|\overline{v}_i|^2}-1\Big). \tag{111}$$

Consider now an arbitrary one-to-one function $\tau=\tau(q)$, such that $q=q(\tau)$ denotes its inverse. It is easy to check that the area of the rectangle $[0,q]\times[0,\tau(q)]$ can be decomposed as follows,

$$q\cdot\tau(q)=\int_0^q\tau(q')\mathrm{d}q'+\int_0^{\tau(q)}q(\tau')\mathrm{d}\tau'. \tag{112}$$

Then, by combining (110), (111) and (112) we obtain

$$\int_0^{\tau}q(\tau')\mathrm{d}\tau'=\sum_{i=1}^{M}\log\left(1+\sqrt{1+p_iq^2}\right) \tag{113}$$
$$=\log\det\big(\mathbf{T}^2(\overline{\boldsymbol{v}},\rho)\big), \tag{114}$$

where the last identity follows from Proposition 1 for $q=q\big(\sqrt{\beta(\overline{\boldsymbol{v}},\rho)}\big)$. Substituting (114) in (108), we obtain an alternative integral form for $\lambda_{\text{su}}(\overline{\boldsymbol{v}},\rho)$,

$$\lambda_{\text{su}}(\overline{\boldsymbol{v}},\rho)=N\int_0^{\sqrt{\beta(\overline{\boldsymbol{v}},\rho)}}q(\tau')\mathrm{d}\tau'-\log\det(\mathbf{I}_N+\rho\mathbf{C}). \tag{115}$$

For small τ, from (34) we obtain $q(\tau)=2\tau+o(\tau)$, which integrates to $\tau^2+o(\tau^2)$. Hence (115) becomes

$$\lambda_{\text{su}}(\overline{\boldsymbol{v}},\rho)=N\beta(\overline{\boldsymbol{v}},\rho)-\log\det(\mathbf{I}_N+\rho\mathbf{C})+o(\beta(\overline{\boldsymbol{v}},\rho)). \tag{116}$$

At low SNR $\mathbf{C}(\rho)=\mathbf{C}+o(\rho)$. Then, it follows that $\beta(\overline{\boldsymbol{v}},\rho)=\frac{1}{N}\overline{\boldsymbol{v}}^H\tilde{\mathbf{Y}}^H\rho\mathbf{C}^*\tilde{\mathbf{Y}}\overline{\boldsymbol{v}}+o(\rho)$. Substituting the low-SNR expansions for $\beta(\overline{\boldsymbol{v}},\rho)$ and using that $\log\det(\mathbf{I}+\rho\mathbf{C})=\rho\,\mathrm{tr}(\mathbf{C})+o(\rho)$ in (116), via (109) we obtain

$$\Lambda_{\text{su}}^{\text{low}}=\max\Big\{0,\lambda_{\max}\big(\tilde{\mathbf{Y}}\mathbf{C}^*\tilde{\mathbf{Y}}^H\big)-\mathrm{tr}\,\mathbf{C}\Big\}. \tag{117}$$

3) Performance analysis: Under Model 2, the GLRT performance depends on the non-centrality parameter

$$\alpha_{\text{su}}=\mathbb{E}\big[2\log T_{\text{su}}\,\big|\,\mathcal{H}_1\big]. \tag{118}$$

Using the property (90) it follows that, for $N\to\infty$,

$$\mathbf{D}^2=\frac{1}{N}\mathrm{diag}\big(\mathbf{Y}\mathbf{Y}^H\big)\;\to\;\mathrm{diag}\left(\boldsymbol{\Sigma}^2+\frac{\mathrm{tr}\,\mathbf{C}^*}{N}\cdot\mathbf{h}\mathbf{h}^H\right). \tag{119}$$

Hence, from the definition of $\mathbf{T}$ in (23), and using the asymptotic consistency of the ML estimator, we obtain

$$t_i^2\;\;\to\;\;1+\frac{\mathrm{tr}\,\mathbf{C}^*}{N}\rho_i, \tag{120}$$

where $\rho_i=\frac{|h_i|^2}{\sigma_i^2}$. Then, substituting (120) in the detector T_{su} in (36)-(37), from the definition (118) we obtain

$$\alpha_{\text{su}}\;\to\;2N\log\frac{\prod_{i=1}^{M}\left(1+\frac{\mathrm{tr}\,\mathbf{C}^*}{N}\rho_i\right)}{\det(\mathbf{I}_N+\rho\mathbf{C})^{\frac{1}{N}}}. \tag{121}$$

Eq. (45) follows using that $\mathrm{tr}\,\mathbf{C}^*=\mathrm{tr}\,\mathbf{C}=N$.

Appendix C
Derivation of (78) for Binary Power Spectrum

For ease of exposition let us define

$$\varrho\doteq\frac{1}{1+\rho\mu}. \tag{122}$$

The optimization in (77) in terms of ρ can be rewritten in terms of ϱ as

$$T_{\text{bs}}=\max_{0<\varrho\le1}\exp\{g(\varrho)\}, \tag{123}$$
$$g(\varrho)\doteq-L\log\left(1-(1-\varrho)b\right)+r\log\varrho. \tag{124}$$

In order to obtain the value of ϱ maximizing (123) we first differentiate $g(\varrho)$,

$$g'(\varrho)\;=\;\frac{-Lb}{1-(1-\varrho)b}+\frac{r}{\varrho}. \tag{125}$$

Equating (125) to 0 we obtain the optimality condition

$$\varrho\;=\;\frac{r(b^{-1}-1)}{L-r}. \tag{126}$$

Given the constraint $0<\varrho\le1$, this condition holds for the optimal value of ϱ in (126) provided that $b\ge r/L$.

On the other hand, for $b<r/L$, we have that

$$g'(\varrho)=\frac{L}{\varrho}\left(\frac{r}{L}-\left(1-\frac{1-b}{1-b+\varrho b}\right)\right) \tag{127}$$
$$\ge\frac{L}{\varrho}\left(\frac{r}{L}-b\right)\ge0, \tag{128}$$

where in (128) we used that $\varrho\le1$ and that $b\le1$ for the detectors in Table II. Therefore, under the stated conditions, $g(\varrho)$ is nondecreasing in $0<\varrho\le1$ and its maximum is attained at $\varrho=1$.

Thus, from (126) (when $b\ge r/L$) and from (127)-(128) (when $0\le b<r/L$), we conclude that the ϱ maximizing (123) is

$$\varrho_\star=\max\left\{1,\;\frac{r(b^{-1}-1)}{L-r}\right\}. \tag{129}$$

Substituting (129) in (123), we obtain (78). The optimal value of ρ in (77) follows from inverting the transformation (122), as $\rho_\star=\frac{1-\varrho_\star}{\mu\varrho_\star}$.

References

[1] E. Axell, G. Leus, E. Larsson, and H. Poor, "Spectrum sensing for cognitive radio: State-of-the-art and recent advances," *IEEE Signal Processing Magazine*, vol. 29, no. 3, pp. 101 – 116, May 2012.

[2] D. Hack, L. Partton, and B. Himed, "Multichannel detection of an unknown rank-one signal with uncalibrated receivers," in *IEEE International Conference on Acoustics, Speech and Signal Processing (ICASSP)*, Florence, Italy, May 2014.

[3] A. Leshem and A. van der Veen, "Multichannel detection and spatial signature estimation with uncalibrated receivers," *Procs. of the 11th IEEE Signal Processing Workshop on Statistical Signal Processing*, pp. 190 – 193, 2001.

[4] A. Leshem and A.-J. van der Veen, "Multichannel detection of Gaussian signals with uncalibrated receivers," *IEEE Signal Processing Lett.*, vol. 8, no. 4, pp. 120–122, April 2001.

[5] A. Taherpour, M. Nasiri-Kenari, and S. Gazor, "Multiple antenna spectrum sensing in cognitive radios," *Wireless Communications, IEEE Transactions on*, vol. 9, no. 2, pp. 814 –823, February 2010.

[6] S. Sedighi, A. Taherpour, and J. Sala, "Spectrum sensing using correlated receiving multiple antennas in cognitive radios," *Wireless Communications, IEEE Transactions on*, vol. 12, no. 11, pp. 5754 – 5766, November 2013.

[7] R. López-Valcarce, G. Vazquez-Vilar, and J. Sala, "Multiantenna spectrum sensing for cognitive radio: overcoming noise uncertainty," in *International Workshop on Cognitive Information Processing (CIP 2010)*, Elba island, Italy, June 2010.

[8] G. Vazquez-Vilar, R. López-Valcarce, and J. Sala, "Multiantenna spectrum sensing exploiting spectral a priori information," *Wireless Communications, IEEE Transactions on*, vol. 10, no. 12, pp. 4345–4355, December 2011.

[9] J. Sala, G. Vazquez-Vilar, and R. López-Valcarce, "Multiantenna GLR detection of rank-one signals with known power spectrum in white noise with unknown spatial correlation," *Signal Processing, IEEE Transactions on*, vol. 60, no. 6, pp. 3065 –3078, June 2012.

[10] I. Akyildiz, W.-Y. Lee, M. Vuran, and S. Mohanty, "A survey on spectrum management in cognitive radio networks," *IEEE Commun. Mag.*, vol. 46, pp. 40–48, Apr. 2008.

[11] J. M. Peha, "Sharing spectrum through spectrum policy reform and cognitive radio," *Proc. IEEE*, vol. 97, pp. 708–719, Apr. 2009.

[12] J. Lundén, V. Koivumen, and H. Poor, "Spectrum exploration and exploitation for cognitive radio: Recent advances," *IEEE Signal Processing Magazine*, vol. 32, no. 3, pp. 123 – 140, May 2012.

[13] S. M. Kay, *Fundamentals of Statistical Signal Processing: Detection Theory*. Englewood Cliffs, N.J.: Prentice-Hall, 1998.

[14] B. C. Levy, *Principles of Signal Detection and Parameter Estimation*. New York: Springer, 2010.

[15] E. Kelly, "An adaptive detection algorithm," *IEEE Transactions on Aerospace and Electronic Systems*, vol. 22, no. 1, pp. 115 – 127, March 1986.

[16] F. Robey, D. Fuhrmann, E. Kelly, and R. Nitzberg, "A CFAR adaptive matched filter detector," *IEEE Transactions on Aerospace and Electronic Systems*, vol. 28, no. 1, pp. 208 – 216, January 1992.

[17] S. Bose and A. Steinhardt, "Adaptive array detection of uncertain rank one waveforms," *IEEE Transactions on Signal Processing*, vol. 44, no. 11, pp. 2801 – 2809, November 1996.

[18] O. Besson, S. Kraut, and L. Scharf, "Detection of an unknown rank-one component in white noise," *IEEE Transactions on Signal Processing*, vol. 54, no. 7, pp. 2835 –2839, July 2006.

[19] P. Wang, J. Fang, N. Han, and H. Li, "Multi-antenna based spectrum sensing for cognitive radios: A GLRT approach," *IEEE Trans. Veh. Technol.*, vol. 59, pp. 1791–1800, May 2010.

[20] D. Ramírez, J. Vía, and I. Santamaría, "Multiantenna spectrum sensing: The case of wideband rank-one primary signals," in *2010 IEEE Sensor Array and Multichannel Signal Processing Workshop*, Israel, October 2010.

[21] D.Ramírez, J.Vía, and I.Santamaría, "The locally most powerful test for multiantenna spectrum sensing with uncalibrated receivers," in *IEEE International Conference on Acoustics, Speech and Signal Processing (ICASSP)*, Kyoto, Japan, March 2012.

[22] S. Ali, D. Ramírez, M. Jansson, G. Seco-Granados, and J. López-Salcedo, "Multi-antenna spectrum sensing by exploiting spatio-temporal correlation," *EURASIP Journal on Advances in Signal Processing*, pp. 1–16, November 2014.

[23] J. Riba, J. Font-Segura, J. Villares, and G. Vázquez, "Frequency-domain GLR detection of a second-order cyclostationary signal over fading channels," *IEEE Transactions on Signal Processing*, vol. 62, no. 8, pp. 1899 – 1912, April 2014.

[24] P. Urriza, E. Rebeiz, and D. Cabric, "Multiple antenna cyclostationary spectrum sensing based on the cyclic correlation significance test," *IEEE Journal on Selected Areas in Communications*, vol. 31, no. 11, pp. 2185 – 2195, November 2013.

[25] ——, "Eigenvalue-based cyclostationary spectrum sensing using multiple antennas," *2012 IEEE Global Communications Conference (Globecom*.

[26] Y. Abramovich, B. Johnson, L. Scharf, A. Pezeshki, and N. Spencer, "Expected likelihood-based detection-estimation of multirank signals," *Forty-Third ASILOMAR conference on signals, systems and computers*, pp. 469 – 471, 2009.

[27] R. Zhang, T. Lim, Y.-C. Liang, and Y. Zeng, "Multi-antenna based spectrum sensing for cognitive radios: A GLRT approach," *IEEE Trans. Commun.*, vol. 58, pp. 84–88, Jan. 2010.

[28] D. Ramírez, G. Vazquez-Vilar, R. López-Valcarce, J. Vía, and I. Santamaría, "Detection of rank-p signals in cognitive radio networks with uncalibrated multiple antennas," *IEEE Trans. Signal Process.*, vol. 59, pp. 3764–3774, Aug. 2011.

[29] D. Hack, C. Rossler, and L. Patton, "Multichannel detection of an unknown rank-n signal using uncalibrated receivers," *IEEE Signal Processing Letters*, vol. 21, no. 8, pp. 998 –1002, August 2014.

[30] J. Tugnait, "On multiple antenna spectrum sensing under noise variance uncertainty and flat fading," *IEEE Transactions on Signal Processing*, vol. 60, no. 4, pp. 1823 – 1832, April 2012.

[31] M. Browne and A. Shapiro, "The asymptotic covariance matrix of sample correlation coefficients under general conditions,," *Linear Algebra Applications*, vol. 83, pp. 169–176, 1986.

[32] "The Gaussian assumption in second-order estimation problems in digital communications," *IEEE Transactions on Signal Processing*, vol. 55, no. 10, pp. 4994 – 5002, October 2007.

[33] D. S. Bernstein, *Matrix Mathematics: Theory, Facts and Formulas (2nd ed.)*. Princeton University Press, 2009.

[34] S. M. Kay, *Fundamentals of statistical signal processing: detection theory*. Englewood Cliffs, NJ: Prentice-Hall, 1998.

[35] R. Steele, *Mobile Radio Communications*. London: Pentech Press, 1992.

[36] S. Lipschutz, M. Spiegel, and J. Liu, *Mathematical Handbook of Formulas and Tables (3rd ed.)*. McGraw-Hill, 2009.